

공학석사 학위논문

증기 폭발에 의한 원자로 하부 헤드의
건전성에 관한 연구

Structural Analysis for the Lower Head of Nuclear Reactor
under In-Vessel Vapor Explosion Loads



지도교수 윤상국

2011 년 2 월

한국해양대학교 대학원

냉동공조공학과 석상균

本 論文을 석상군의 工學碩士 學位論文으로 認准함



2011 년 2 월 23 일

한국해양대학교 대학원

Content

Abstract	i
List of Tables	iii
List of Figures	iv
1. Introduction	1
1.1 The reason to cause failure of reactor vessel	1
1.2 Two kinds of failures of reactor vessel	1
1.2.1 Alpha-mode containment failure	1
1.2.2 Lower head failure	1
2. Analysis procedure of lower head failure	3
2.1 Introduction.....	3
2.2 Safety assessment process.....	3
2.3 Analysis of in-vessel explosion.....	4
2.4 Analysis method using ANSYS program.....	5
2.4.1 Static analysis of ANSYS.....	6
2.4.2 Transient analysis of ANSYS	7
2.5 Failure criteria.....	17
2.5.1 Design criteria	17
2.5.2 Structural failure criteria	17
2.5.3 Boiling failure criteria	18
2.5.4 Thermal failure criteria.....	19
3. Structural analysis procedure and results	20

3.1 Structural analysis of 2-D modeling lower head.....	20
3.1.1 Stress analysis under design condition.....	20
3.1.2 Transient dynamic analysis of explosion load.....	22
3.1.3 Results of simplified 2-D model structural analysis.....	22
3.1.3.1 Stress analysis results under design condition.....	22
3.1.3.2 Transient dynamic analysis of explosion load results.....	23
3.2 Structural analysis of 3-D model lower head.....	41
3.2.1 Stress analysis under design condition.....	41
3.2.2 Transient dynamic analysis of explosion load.....	41
3.2.3 Results of 3-D modeling structural analysis.....	41
3.2.3.1 Stress analysis results under design condition.....	41
3.2.3.2 Transient dynamic analysis of explosion load results.....	42
3.3 Thermal Analysis.....	55
3.3.1 Introduction.....	55
3.3.3 Thermal analysis results.....	56
3.4 Thermo-mechanical analysis for 2-D modeling.....	58
3.4.1 Thermo-mechanical analysis under design condition.....	58
3.4.2 Thermo-mechanical analysis under transient dynamic of explosion load...58	58
3.4.3 Results of thermo-mechanical analysis.....	59
3.4.3.1 Thermo-mechanical analysis results under design condition.....	59
3.4.3.2 Thermo-mechanical analysis results under transient dynamic of explosion load.....	59
4. Conclusion and Future Work.....	73
References.....	75

Structural Analysis for the Lower Head of Nuclear Reactor under In-Vessel Vapor Explosion Loads

Xi Shangjun

Department of Refrigeration Engineering, Graduate College,
Korea Maritime University

Abstract

The objective of this paper is to assess the lower head of nuclear reactor under the in-vessel vapor explosion load. Firstly, the calculated explosion pressure loads are applied on the lower head inner wall for 2-D model and 3-D model, respectively, to calculate the equivalent strain and membrane stress intensity; secondly, both calculated explosion pressure loads and thermal loads are imposed on the 2-D model of the lower head to calculate the equivalent strain, membrane stress intensity, and total mechanical and thermal strain. Then, the calculated strain and stress results are compared with the reference standard values of failure criteria to determine the failure probability of the lower head. All the strain and stress calculations are performed by ANSYS 11.0 Program.

The structure analysis results show that the lower head failure does not exist under the pressure value up to 118.5 MPa in vessel explosion.

The thermo-mechanical results show that the lower head failure under the pressure value up to 118.5 MPa and temperature value up to 700°C in-vessel explosion also does not exist. During this analysis process, the nucleate boiling crisis will not occur when the

outside wall of lower head is cooled by the saturation water at 100°C and 0.1 MPa.



List of Tables

Table 1 Loading data for 2-D model structural analysis under design condition

Table 2 Mechanical properties of material at 260°C for 2-D model structural analysis

Table 3 Loading data for 2-D model structural analysis under transient explosion

Table 4 Summary of 2-D modeling structural analysis results

Table 5 Summary results of 3-D modeling structural analysis

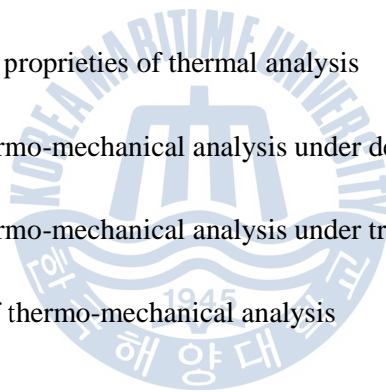
Table 6 Loading data for thermal analysis

Table 7 Material mechanical properties of thermal analysis

Table 8 Loading data for thermo-mechanical analysis under design condition

Table 9 Loading data for thermo-mechanical analysis under transient explosion

Table 10 Summary results of thermo-mechanical analysis



List of Figures

Fig. 1 Safety Analysis process of lower head

Fig. 2 Schematic of reactor vessel

Fig. 4 Top view of lower head

Fig. 5 Schematic of pipe

Fig. 6 Simplified 2-D model of lower head for structural analysis

Fig. 7 Finite element simplified 2-D model of lower head for structural analysis

Fig. 8 3-D Model of lower head for structural analysis

Fig. 9 Finite element 3-D model of lower head for structural analysis

Fig. 10 Simplified 2-D model of lower head for thermal analysis

Fig. 11 Finite element simplified 2-D model of lower head for thermal analysis

Fig. 12 ANSYS element description used in mechanical analysis

Fig. 13 ANSYS element description used in thermo-mechanical analysis

Fig. 14 The result appropriate for quantifying the thermal failure criteria

Fig. 15 Time history of explosion pressure in case of starting explosion at the bottom of head

Fig. 16 Time history of explosion pressure in case of starting explosion at the top of Head

Fig. 17 Time history of explosion pressure in case of single jet mixing

Fig. 18 Input time history of explosion pressure applied uniformly on the whole inside of the head (CASE 1)

Fig. 19 Pressure loaded locations of lower head for CASE 1

Fig. 20 Input time history of explosion pressure applied on 6 segments of inside of the head (CASE 2)

Fig. 21 Pressure loaded locations of lower head for CASE 2

Fig. 22 Input time history of explosion pressure applied uniformly in case of single jet mixing (CASE 3).

Fig. 23 Pressure loaded locations of lower head for CASE 3

Fig. 24 Stress intensity distribution of 2-D model structural analysis under design condition

Fig. 25 Equivalent strain distribution of 2-D model structural analysis under design condition

Fig. 26 Path 1 of 2-D model structural analysis under design condition

Fig. 27 Membrane and membrane plus bending stress along Path 1 of 2-D model structural analysis under design condition

Fig. 28 Stress intensity distribution at 0.01 sec of 2-D model structural analysis for CASE 1

Fig. 29 Equivalent strain distribution at 0.01 sec of 2-D model structural analysis for CASE 1

Fig. 30 Path 1 and Node A of 2-D model structural analysis for CASE 1

Fig. 31 Membrane and membrane plus bending stress at 0.01 sec along Path 2 of 2-D model structural analysis fro CASE 1

Fig. 32 Time history of equivalent stress at Node A of 2-D model structural analysis for CASE 1

Fig. 33 Time history of equivalent strain at Node A of 2-D model structural analysis for CASE 1

Fig. 34 Stress intensity distribution at 0.01 sec of 2-D model structural analysis for CASE 2

Fig. 35 Equivalent strain distribution at 0.01 sec of 2-D model structural analysis for CASE 2

Fig. 36 Path 1 and Node A of 2-D model structural analysis for CASE 2

Fig. 37 Membrane and membrane plus bending stress at 0.01 sec along Path 3 of 2-D model structural analysis for CASE 2

Fig. 38 Time history of equivalent stress at Node B of 2-D model structural analysis for CASE 2

Fig. 39 Time history of equivalent strain at Node B of 2-D model structural analysis for CASE 2

Fig. 40 Stress intensity distribution at 0.0072 sec of 2-D model structural analysis for CASE 3

Fig. 41 Equivalent strain distribution at 0.0072 sec of 2-D model structural analysis for CASE 3

Fig. 42 Path 1 and Node A of 2-D model structural analysis for CASE 3

Fig. 43 Membrane and membrane plus bending stress at 0.0072 sec along Path 4 of 2-D model structural analysis for CASE 3

Fig. 44 Time history of equivalent stress at Node C of 2-D model structural analysis for CASE 3

Fig. 45 Time history of equivalent strain at Node C of 2-D model structural analysis for CASE 3

Fig. 46 Stress intensity distribution of 3-D model structural analysis under design Condition

Fig. 47 Equivalent strain distribution of 3-D model structural analysis under design Condition

Fig. 48 Path 1 of 3-D model structural analysis under design condition

Fig. 49 Membrane and membrane plus bending stress along Path 5 of 3-D model

structural analysis under design condition

Fig. 50 Stress intensity distribution at 0.01 sec of 3-D model structural analysis for CASE 1

Fig. 51 Equivalent strain at 0.01 sec of 3-D model structural analysis for CASE 1

Fig. 52 Path 1 and Node A of 3-D model structural analysis for CASE 1

Fig. 53 Membrane and membrane plus bending stress at 0.01 sec along Path 6 of 3-D model structural analysis for CASE 1

Fig. 54 Time history of equivalent stress at Node D of 3-D model structural analysis for CASE 1

Fig. 55 Time history of equivalent strain at Node D of 3-D model structural analysis for CASE 1

Fig. 56 Stress intensity distribution at 0.01 sec of 3-D model structural analysis for CASE 2

Fig. 57 Equivalent strain distribution at 0.01 sec of 3-D model structural analysis for CASE 2

Fig. 58 Path 1 and Node A of 3-D model structural analysis for CASE 2

Fig. 59 Membrane and membrane plus bending stress at 0.01 sec along Path 1 of 3-D model structural analysis for CASE 2

Fig. 60 Time history of equivalent stress at Node A of 3-D model structural analysis for CASE 2

Fig. 61 Time history of equivalent strain at Node A of 3-D model structural analysis for CASE 2

Fig. 62 Stress intensity distribution at 0.0072 sec of 3-D model structural analysis for CASE 3

Fig. 63 Equivalent strain distribution at 0.0072 sec of 3-D model structural analysis for CASE 3

Fig. 64 Path 1 and Node A of 3-D model structural analysis for CASE 3

Fig. 65 Membrane and membrane plus bending stress at 0.0072 sec along Path 8 of 3-D model structural analysis for CASE 3

Fig. 66 Time history of equivalent strain at Node F of 3-D model structural analysis for CASE 3

Fig. 67 Time history of equivalent strain at Node F of 3-D model structural analysis for CASE 3

Fig. 68 Temperature distribution of 2-D model of lower head

Fig. 69 Thermal flux distribution of 2-D model of lower head

Fig. 70 Stress intensity distribution of 2-D model thermo-mechanical analysis under design condition

Fig. 71 Total strain distribution of 2-D model thermo-mechanical analysis under design condition

Fig. 72 Path 1 of 2-D model thermo-mechanical analysis under design condition

Fig. 73 Membrane and membrane plus bending stress along Path 9 of 2-D model thermo-mechanical analysis under design condition

Fig. 74 Stress intensity distribution at 0.01 sec of 2-D model thermo-mechanical analysis for CASE 1

Fig. 75 Total strain distribution at 0.01 sec of 2-D model thermo-mechanical analysis for CASE 1

Fig. 76 Path 1 and Node A of 2-D model thermo-mechanical analysis for CASE 1

Fig. 77 Membrane and membrane plus bending stress at 0.01 sec along Path 10 of 2-D model thermo-mechanical analysis for CASE 1

Fig. 78 Time history of equivalent stress at Node G of 2-D model thermo-mechanical analysis for CASE 1

Fig. 79 Time history of equivalent strain at Node G of 2-D model thermo-mechanical analysis for CASE 1

Fig. 80 Stress intensity distribution at 0.01 sec of 2-D model thermo-mechanical analysis for CASE 2

Fig. 81 Total strain distribution at 0.01 sec of 2-D model thermo-mechanical analysis under CASE 2

Fig. 82 Path 1 and Node A of 2-D model thermo-mechanical analysis for CASE 2

Fig. 83 Membrane and membrane plus bending stress at 0.01 sec along Path 11 of 2-D model thermo-mechanical analysis for CASE 2

Fig. 84 Time history of equivalent stress at Node H of 2-D model thermo-mechanical analysis for CASE 2

Fig. 85 Time history of equivalent strain at Node H of 2-D model thermo-mechanical analysis for CASE 2

Fig. 86 Stress intensity distribution at 0.0072 sec of 2-D model thermo-mechanical analysis for CASE 3

Fig. 87 Total strain distribution at 0.0072 sec of 2-D model thermo-mechanical analysis for CASE 3

Fig. 88 Path 1 and Node A of 2-D model thermo-mechanical analysis for CASE 3

Fig. 89 Membrane and membrane plus bending stress at 0.0072 sec along Path 12 of 2-D model thermo-mechanical analysis for CASE 3

Fig. 90 Time history of equivalent stress at Node I of 2-D model thermo-mechanical analysis for CASE 3

Fig. 91 Time history of equivalent strain at Node I of 2-D model thermo-mechanical analysis for CASE 3

1. Introduction

1.1 The reason to cause failure of reactor vessel

In the light water reactors, if complete and prolonged failure of normal and emergency coolant flow occurs, fission product decay heat could cause melting of the reactor fuel. If the molten fuel mass accumulates it may relocate into reactor lower plenum and if the lower head fails it may eventually be brought into the fuel-coolant interactions (FCI) arises as the core melt relocates into water pool in-vessel as well as ex-vessel and also, as a consequence of implementing accident management strategies involving water addition to a degraded or molten core[1].

In general, the FCI process involves transfer of heat from the molten fuel to the surrounding coolant in a time scale ranging from milliseconds range can lead to energetic vapor explosions which, if enough energetic, may challenge reactor vessel and containment integrity thereby posing a radiological risk to the environment.

1.2 Two kinds of failures of reactor vessel

1.2.1 Alpha-mode containment failure

If the amount of melt involved in a vapor explosion inside the reactor vessel is large enough and the resulting energy conversion of the melt heat to mechanical energy is sufficiently large, the explosion may fail the reactor upper head, throwing it upward, hitting the containment ceiling, consequently posing a potential risk of releasing failure (α -mode failure). For years reactor safety analysts have studied the probability of the α -mode containment failure and have reached a tentative consensus on that the α -mode containment failure is not risk significant.

1.2.2 Lower head failure

The in-vessel retention (IVR) strategy, employed in advanced light water reactors (ALWR) with passive design features, is based upon external cooling of the reactor heat from the vessel wall thereby assuring its integrity from a combined thermo-mechanical static loading imparted by the hot core debris inside. To assure the success of the IVR strategy, the potential for an early failure of the lower head from in-vessel vapor explosions must be ruled out. Also, one notes that in event the lower head fails, the resulting event may create an opportunity for the wide spectrum of ex-vessel severe accident phenomena including direct containment heating and ex-vessel FCI.

This new accident management strategy of in-vessel retention in advanced light water reactors has directed the risk potential of in-vessel vapor explosions from the α -mode containment failure to the reactor lower head failure.

The objective of the present study is to perform a safety assessment of the reactor lower head integrity of nuclear reactor under the potential in-vessel vapor explosion loads. The initial conditions of melt relocation into the lower plenum were provided by the bounding approximation in order to provide conservative results.

2. Analysis procedure of lower head failure

2.1 Introduction

The paper is to develop a methodology for assessing likelihood of lower head failure under millisecond-duration pressure pulses with peaks in the kilobar range. It is very important to characterize and understand the dynamics due to axisymmetrically distributed highly transient loads to strain hardening effects on material constitutive behavior.

2.2 Safety assessment process

The process of the safety assessment of the reactor vessel lower head integrity under in-vessel vapor explosion is shown in Fig. 1.

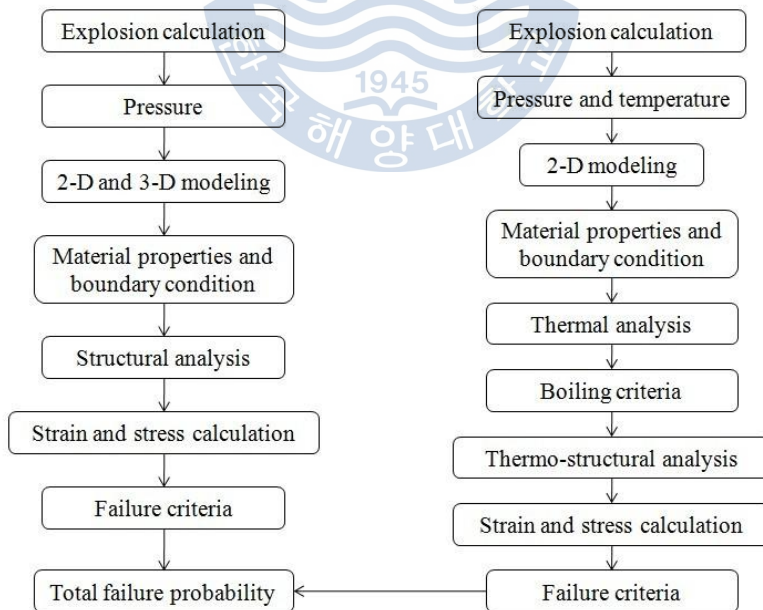


Fig. 1 Safety Analysis process of lower head

The explosion calculations were performed using TRACER-II code[1], then can

obtain the pressure load and thermal load. The structural analysis process is: using the calculated explosion pressure imposed on the lower head inner wall, strain and stress calculation were performed using ANSYS program, and then comparing the calculated value with the allowable failure criteria value to determine the failure probability of the lower head. The thermal analysis process is: using the calculated explosion temperature imposed on the lower head inner wall and the convection boundary condition imposed on the lower head out wall, temperature distribution and heat flux performed using ANSYS program, then comparing the calculate heat flux value with the allowable boiling failure criteria value to determine the boiling failure probability. The thermo-structural analysis process is: using the calculated explosion pressure and the thermal analysis result applied on the lower head inner wall, total strain (total mechanical and thermal strain) and stress were also performed by ANSYS program, then comparing the calculated value with the allowable failure criteria value to determine the failure probability of the lower head.

2.3 Analysis of in-vessel explosion

To assess the integrity of reactor vessel under in-vessel vapor explosion, the calculation of pressure produced by vapor explosion is essential firstly.

The purpose of in-vessel vapor explosion analysis is to provide dynamic pressure impulses imposed on the inner wall of lower head for the strain analysis. In order to provide a conservative results, two groups of calculations were performed; (1) under the assumption of uniform premixture throughout the lower plenum, explosion calculations were performed with the variation of trigger position and magnitude, and fuel and vapor volume fractions within the range of physically realistic bounds. (2) a single jet melt enters lower plenum filled with coolant. In this case, premixing and subsequent explosion propagation calculations were performed with the variation of triggering time after the

melt entry.

The calculation of equation pressure were performed using TRACER-II code by professor Bang[1]. Time histories of explosion pressure when explosion starts at the bottom and top of the lower head in Fig. 15 and Fig. 16 respectively, a time history of explosion in case if single jet mixing is shown in Fig. 17. In this paper, the calculation results are used directly.

2.4 Analysis method using ANSYS program

In the paper, two analysis methods are used: static analysis method and transient analysis method. For static method, design pressure 17.24 MPa is used to analyse, and for the transient method, three cases explosion dynamic pressure are used analyse. For modeling, two models are used to analysis the possibility of lower head failure, one is simplified 2-D modeling, the another is 3-D modeling. The schematic view of the lower plenum of nuclear reactor is shown in Fig. 2, the lower plenum is occupied by lower support structure and in-core instrumentation guide tubes. Fig. 3 is the front view of lower head, Fig. 4 is the top view of lower head, Fig. 5 is the schematic of support pipe.

In this study, it is assumed that the lower plenum is empty, hemispherical only for the simplified 2-D modeling, and only the support pipe is considered for the 3-D modeling.

The geometric modeling of the lower head is performed by ANSYS 11.0, for structural analysis, using PLANE 42 solid element and SOLID 185 element (Fig. 12) to model the 2-D modeling head and 3-D modeling head respectively, as shown in from Fig. 6 to Fig. 9; for 2- D modeling thermal analysis, using thermal PLANE 55 element (Fig. 13) to model the lower head, as shown in Fig. 10 and Fig. 11; for 2-D thermo-mechanical analysis, using PLANE 42 solid element to model the lower head, as shown in Fig. 6 and Fig. 7.

In the analysis process, there are four processes: firstly, apply the static pressure and

transient pressure for the 2-D modeling; secondly, apply the static pressure and transient pressure for the 3-D modeling; thirdly, apply the temperature for the 2-D modeling, at last, apply the thermal result from the thirdly process and the static pressure and transient pressure for the 2-D modeling.

Comparing the ANSYS calculated results with the failure criteria to confirm whether the possibility of lower head failure occurs or not under vapor explosion load and thermal load.

2.4.1 Static analysis of ANSYS

The static analysis solution method is valid for all degrees of freedom (DOFs). Inertial and damping effects are ignored, except for static acceleration fields.

The overall equilibrium equations

$$[K]\{u\} = \{F^a\} + \{F^r\} \quad (2-1)$$

where:

$$[K] = \text{total stiffness matrix} = \sum_{m=1}^N [K_e]$$

$\{u\}$ = nodal displacement vector

N = number of elements

$[K_e]$ = element stiffness matrix

$\{F^r\}$ = reaction load vector

$\{F^a\}$, the total applied load vector, is defined by:

$$\{F^a\} = \{F^{nd}\} + \{F^{ac}\} + \sum_{m=1}^N (\{F_e^{th}\} + \{F_e^{pr}\}) \quad (2-2)$$

where

$\{F^{nd}\}$ = applied nodal load vector

$\{F^{ac}\} = - [M] \{a_c\}$ = acceleration load vector

$[M]$ = total mass matrix = $\sum_{m=1}^N [M_e]$

$[M_e]$ = element mass matrix (described in Derivation of Structural Matrices)

$\{a_c\}$ = total acceleration vector (defined in Acceleration Effect)

$\{F_e^{th}\}$ = element thermal load vector (described in Derivation of Structural Matrices)

$\{F_e^{pr}\}$ = element pressure load vector (described in Derivation of Structural Matrices)

$$\{Q^a\} = \{Q^{nd}\} + \sum_{m=1}^N \{Q_e\} \quad (2-3)$$

2.4.2 Transient analysis of ANSYS

The transient analysis solution method used depends on the DOFs involved. Structural, acoustic, and other second order systems (that is, the systems are second order in time) are solved using one method and the thermal, magnetic, electrical and other first order systems are solved using another. Each method is described subsequently. If the analysis contains both first and second order DOFs (e.g. structural and magnetic), then each DOF is solved using the appropriate method. For matrix coupling between first and second order effects such as for piezoelectric analysis, a combined procedure is used. The transient dynamic equilibrium equation of interest is as follows for a

linear structure:

$$[M]\{\ddot{u}\} + [C]\{\dot{u}\} + [K]\{u\} = \{F^a\} \quad (2-4)$$

where:

$[M]$ = structural mass matrix

$[C]$ = structural damping matrix

$[K]$ = structural stiffness matrix

$\{\ddot{u}\}$ = nodal acceleration vector

$\{\dot{u}\}$ = nodal velocity vector

$\{u\}$ = nodal displacement vector

$\{F^a\}$ = applied load vector

There are two methods in the ANSYS program which can be employed for the solution of the linear: the forward difference time integration method and the Newmark time integration method. The forward difference method is used for explicit transient analyses and is described in the LS-DYNA Theoretical Manual.



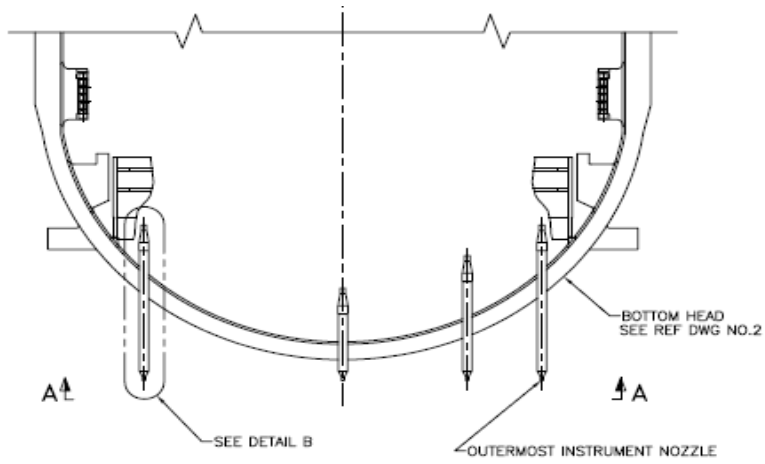


Fig. 3 Front view of lower head

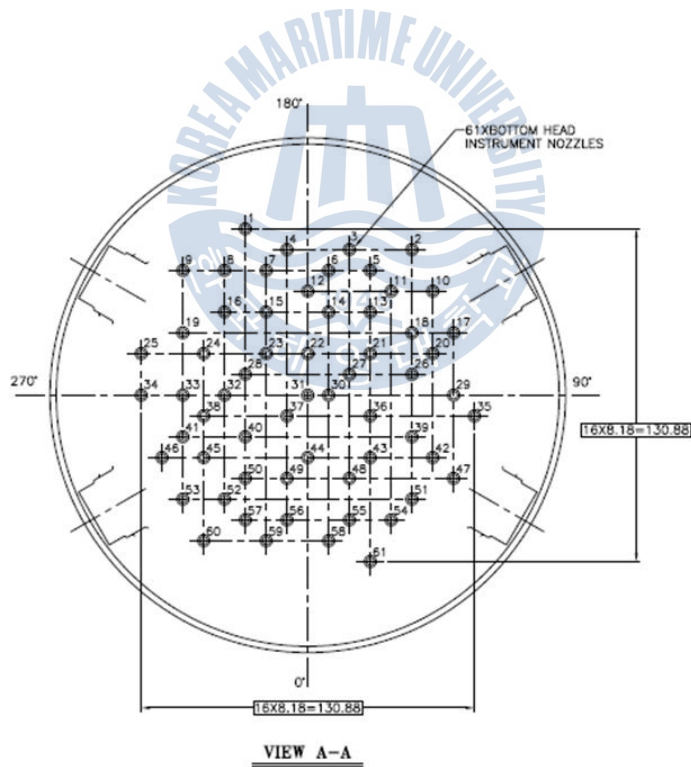


Fig. 4 Top view of lower head

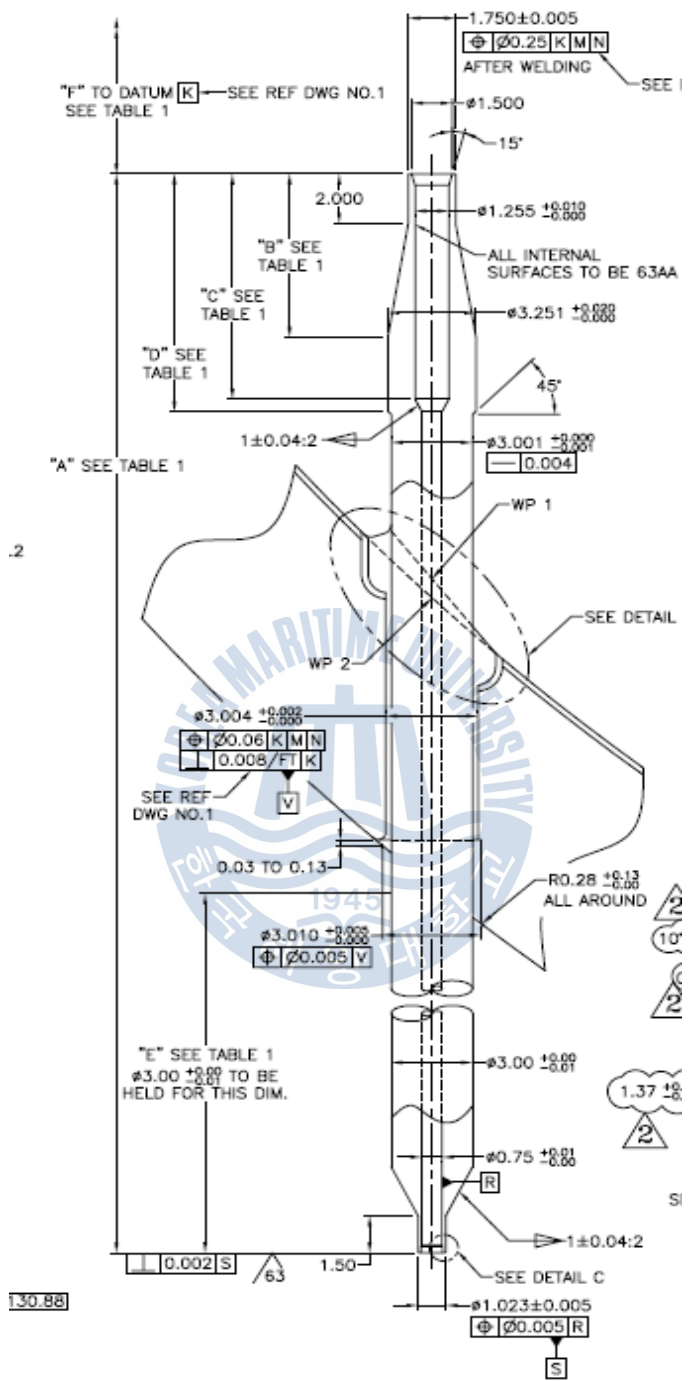


Fig. 5 Schematic diagram of pipe

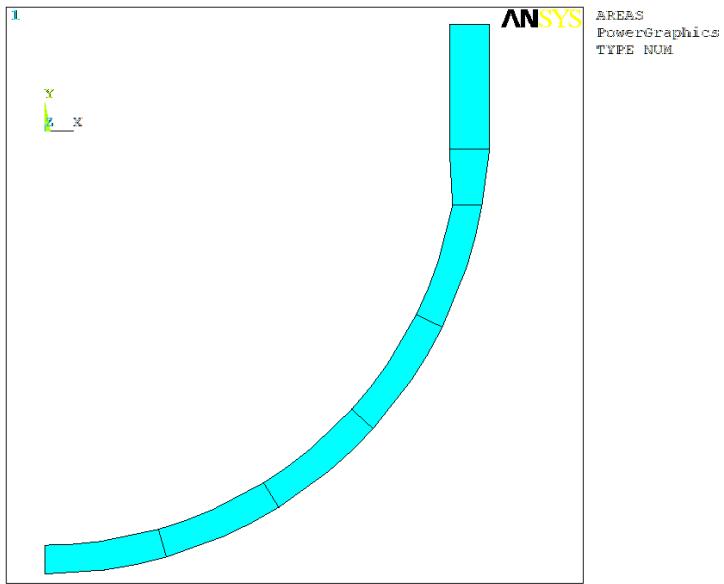


Fig. 6 Simplified 2-D model of lower head for structural analysis

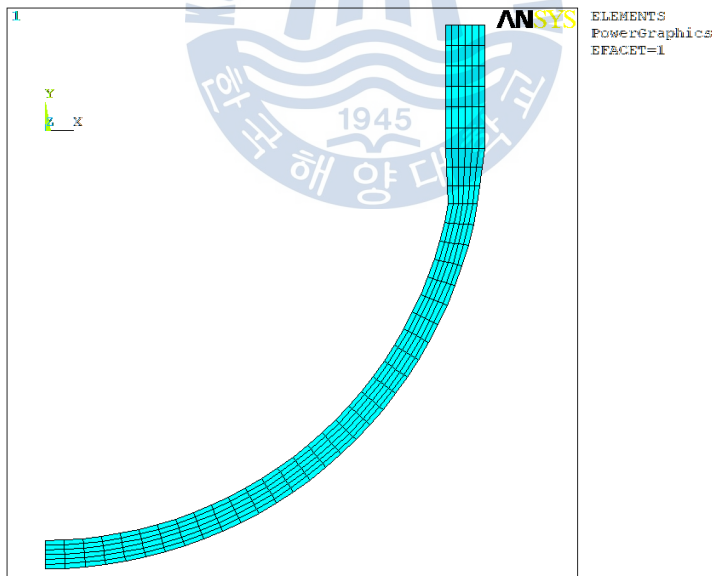


Fig. 7 Finite element simplified 2-D model of lower head for structural analysis

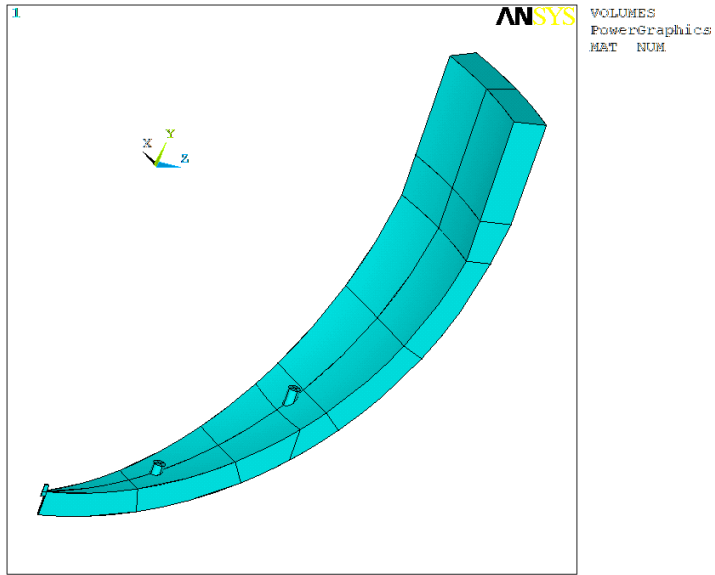


Fig. 8 3-D Model of lower head for structural analysis

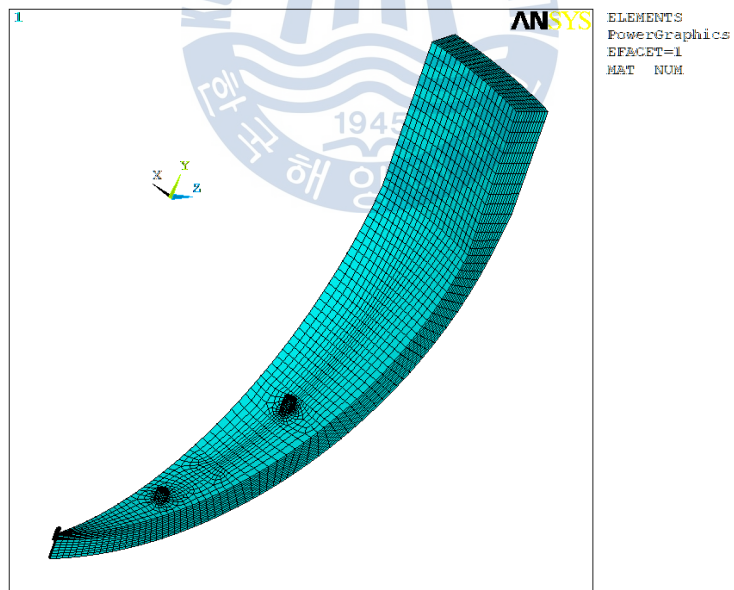


Fig. 9 Finite element 3-D model of lower head for structural analysis

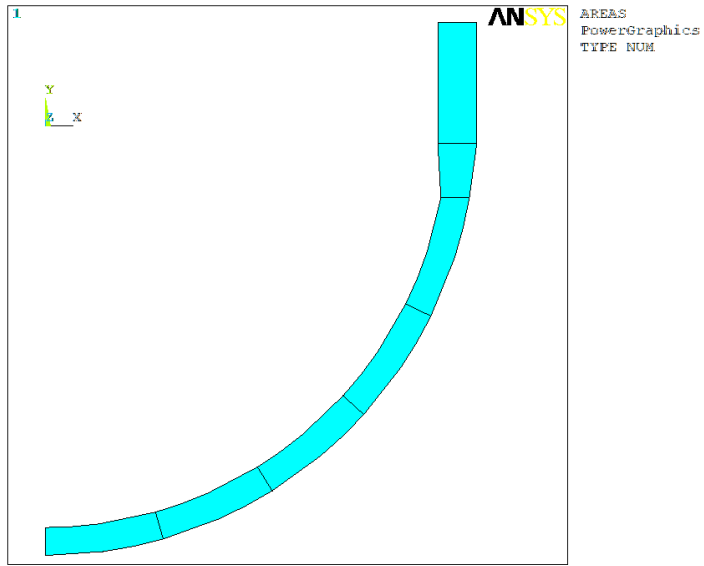


Fig. 10 Simplified 2-D model of lower head for thermal analysis

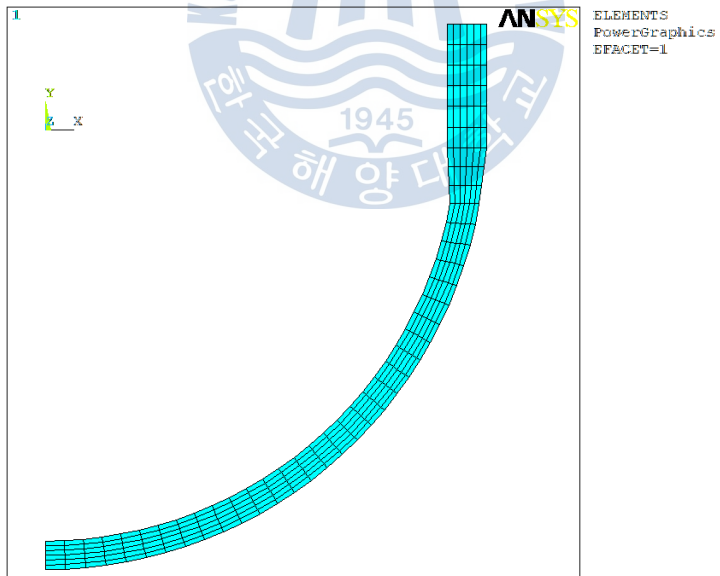
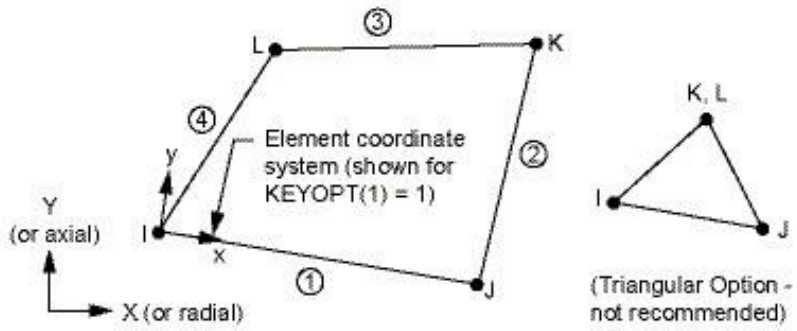
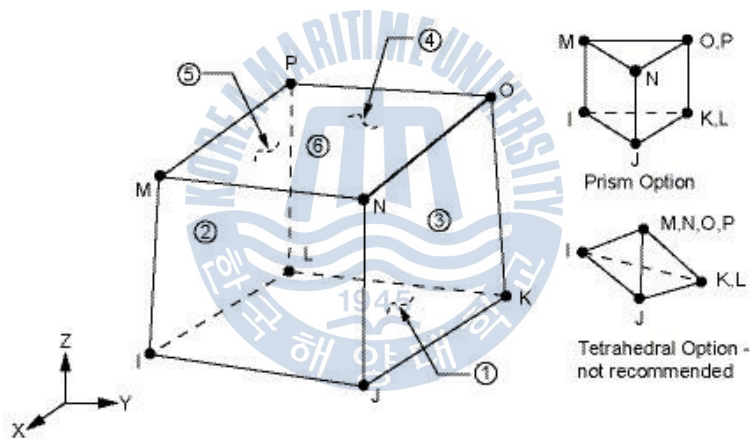


Fig. 11 Finite element simplified 2-D model of lower head for thermal analysis

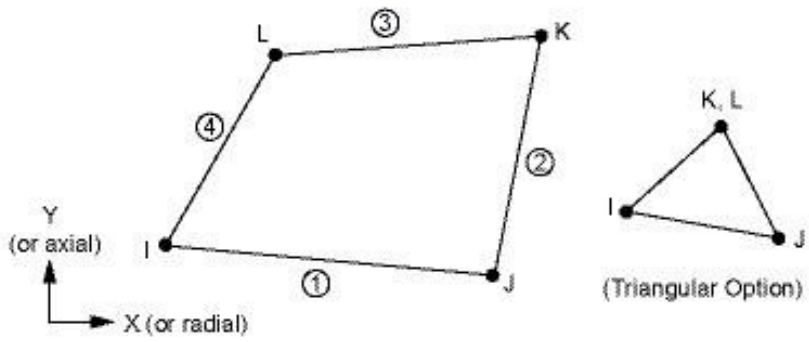


(a) Structural PANE 42 geometry in ANSYS

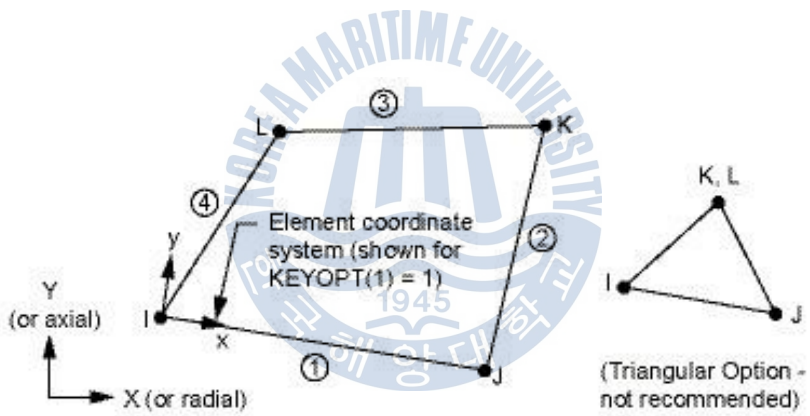


(b) Structural SOLID 185 geometry in ANSYS

Fig. 12 ANSYS element description used in mechanical analysis



(c) Thermal PLANE 55 geometry in ANSYS



(d) Structure PLANE 42 geometry in ANSYS

Fig. 13 ANSYS element description used in thermo-mechanical analysis

2.5 Failure criteria

2.5.1 Design criteria

The design criteria are based on ASME Boiler & Pressure Vessel Design Code Section III NB-3200[2]. A detailed stress analysis of all major structural components shall be prepared in sufficient detail to show that each of the stress limitations of NB-3220 and NB-3230 is satisfied when the component is subjected to loading of NB-3110.

The allowable value of general primary membrane stress intensity is S_m at the design temperature. The primary membrane plus primary bending stress intensity is derived from the highest value across the thickness of a section of the general or local primary membrane stress plus primary bending stress produced by design pressure and other specified design mechanical loads, but excluding all secondary and peak stresses. For solid rectangular sections, the allowable value of this intensity is $1.5S_m$ [1].

2.5.2 Structural failure criteria

Failure criteria used by Bohl and Butler[3] as well as by Berman et al.[4] were phenomenologically based on continuum mechanics. Each criterion based on failure on equivalent plastic strain $\bar{\epsilon}_p$, which is defined in terms of the principal plastic strains by

$$\bar{\epsilon}_p = \frac{\sqrt{2}}{3} \left[(\epsilon_1 - \epsilon_2)^2 + (\epsilon_2 - \epsilon_3)^2 + (\epsilon_3 - \epsilon_1)^2 \right] \quad (2-5)$$

According to Bohl and Butler, failure should occur at -12% equivalent plastic strain. Berman et al. on the other hand, placed this criterion at -18%.

According to criterion of Ghosh, which is metallurgically based in rupture, failure occurs when

$$\epsilon_{pg} \leq \epsilon_{p\max} \quad (2-6)$$

Where is the maximum principle plastic strain and if the failure plastic strain obtained from

$$\varepsilon_{pg} = 126.1 \left[\frac{1 + \beta^2 - 1.2\beta}{1 + \beta} \right] (1 + \delta^2 + 1.2\delta)^{-0.5} \quad (2-7)$$

Where and are defined as

$$\beta = \frac{1.5 + 2.5\delta}{2.5 + 1.5\delta} \quad \delta = \frac{\varepsilon_1}{\varepsilon_2} \quad (2-8)$$

The failure obtained using this criterion were at the same location but somewhat delayed in relation to those obtained using the 12% or 18% criterion discussed previously.

Here, choose 11% as the criteria.

2.5.3 Boiling failure criteria

Nucleate boiling heat transfer coefficients are so high that any flux level, up the CHF, can be accommodated with only a few tens of degrees in wall superheat (temperature above the coolant saturation temperature). Nominally, therefore, in nucleate boiling the outer surface of the lower head is at 100°C (note that the vessel wall will cool from the inside during depressurization of the reactor coolant system, so that nucleate boiling will occur without any delay when the lower head comes in contact with cavity water on the outside). This is very significant for the structural stability of the lower head.

The most limiting failure mechanism of the lower head is the boiling crisis. It occurs when the heat flux through it exceeds the critical heat flux at the same location, and it results in sudden transition of the flow regime from nucleate to film boiling. Film boiling is characterized by considerably lower heat transfer coefficients, and as a consequence the surface temperature rises to considerably higher values in order to accommodate the imposed thermal load from the inside. For example, for a heat flux of 400 kW/m² the

surface temperature must rise to about 1200°C in saturated water. At such temperature the steel loses essentially all of its strength, and it becomes susceptible to creep, and structural instability, even and the modest mechanical loads of interest to this problem.

So, in boiling heat transfer problems, must control the heat flux seriously, according to the experiment results conducted by T.G. Theofanous and C. Liu et al.[6], Fig. 17 is the result appropriate for quantifying the thermal failure criteria, if the heat flux don't exceed the values in the Fig. 17, the boiling crisis will not occur.

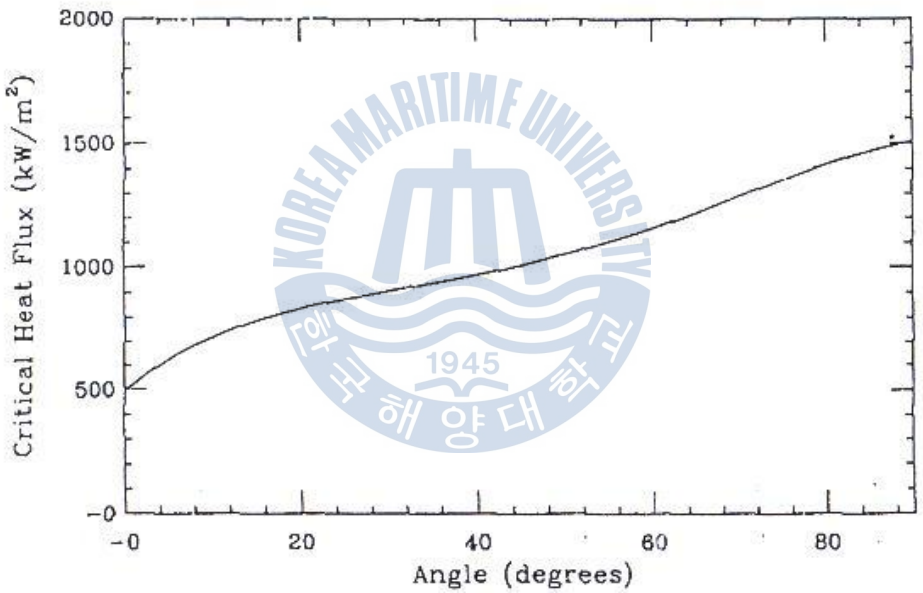


Fig. 14 The result appropriate for quantifying the thermal failure criteria

2.5.4 Thermal failure criteria

Vessel failure can be initiated either by plastic instability or creep mechanisms. When the membrane stress exceeds the material strength (which reduces significantly with increasing temperature) plastic deformation occurs. Creep is an active deformation mechanism at temperature above 630°C. When the temperature reaches a higher value

through the complete wall thickness then creep deformation can occur even at low pressure[8].

For plastic deformation, the membrane stress and the membrane plus bending stress from the highest value across the thickness of a section of the general or local primary membrane stress plus primary bending stress produced by design pressure and other specified design mechanical loads, but excluding all secondary and peak stresses. For solid rectangular sections, the allowable value of the intensity is $1.5 S_m$.

For creep deformation criteria, according to experiment, if the total strain (total mechanical and thermal strain) is less than 6%, it will be safe[7].



3. Structural analysis procedure and results

In this paper, using the ANSYS program to perform the analysis procedure, including the 2-D modeling and 3-D modeling structural analysis, 2-D modeling thermal analysis and thermo-structural analysis.

3.1 Structural analysis of 2-D modeling lower head

For this analysis, there are two situations: static analysis and transient analysis, both using the calculated explosion pressure imposed on the lower head inner wall, strain and stress calculation were performed using ANSYS program, and then comparing the calculated value with the allowable failure criteria value to determine the failure probability of the lower head.

3.1.1 Stress analysis under design condition

The design condition pressure of 17.24 MPa is applied for the inner side of the head.

Material of the lower head is SA508 class 3 steel

Table 1 Loading data for 2-D model structural analysis under design condition

Loadings	Data
Pressure load	17.24 MPa

Table 2 Mechanical properties of material at 260°C for 2-D model structural analysis

Properties	Young's modulus	Poisson's ratio	Density	Yield strength
------------	-----------------	-----------------	---------	----------------

	(GPa)		(Kg / m ³)	(MPa)
Value	172.2	0.312	8110	422

3.1.2 Transient dynamic analysis of explosion load

Time histories of explosion pressure when explosion starts at the bottom and top of the lower head are shown in Fig. 15 and Fig. 16, respectively. A time history of explosion in case of single jet mixing is shown in Fig.17. But these are too complex to take input data of ANSYS. Simplified input data are shown in from Fig.18, Fig.20 and Fig. 22.

For CASE 1, explosion pressure applies uniformly on the whole inside of the lower head. For CASE 2, the inside surface of the head is divided by 7 segments, and various history of explosion pressure applied on the each segments. For CASE 3, the inside surface of the head is divided by 3 segments, and various history of explosion pressure applies on the each segments.

Table 3 Loading data for 2-D model structural analysis under transient explosion

Loadings	Data
Pressure load	As shown in Fig. 18, Fig. 20 and Fig. 22

3.1.3 Results of simplified 2-D model structural analysis

There are two situations: results under design condition and transient dynamic explosion load.

3.1.3.1 Stress analysis results under design condition

A contour plot of the stress intensity is shown in Fig. 24, the maximum stress intensity is 190.39 MPa at junction of the top of the head and the shell. A plot of sections tresses

across the wall thickness of a section is shown in Fig 27, the maximum membrane stress intensity is 123.83 MPa, which is less than the allowable value of 204 MPa; the maximum membrane plus bending stress intensity is 171.61 MPa, which is less than the allowable value of 306 MPa. The equivalent strain distribution is shown in Fig.25, the maximum equivalent strain is 0.0997% and is much less than the allowable value of 11%.

3.1.3.2 Transient dynamic analysis of explosion load results

For CASE 1, at the last step 0.01 sec, the stress intensity distribution and equivalent strain distribution are shown in Fig. 28 and Fig. 29, respectively, the maximum equivalent strain is 0.0975%, which much less than the allowable value 11%. The membrane stress and membrane plus bending stress along path 2 is plotted in Fig. 30, the maximum membrane stress is 126.99 MPa and is less than the allowable value 204 MPa; the maximum membrane plus bending stress is 145.66 MPa and is less than the allowable value 306 MPa. Time history of equivalent strain and stress at node A are shown in Fig. 32 and Fig. 33, respectively, both the value increase with time, but the value is very small.

For Case 2, at the last step 0.01 sec, the stress intensity distribution and equivalent strain distribution are plotted in Fig. 34 and Fig. 35, respectively, the maximum equivalent strain is 0.1155% and is less than the allowable value 11%. The membrane stress and membrane plus bending stress along path 3 is plotted in Fig. 37, the maximum membrane stress is 140.05 MPa, which is less than the allowable value 204 MPa; the maximum membrane plus bending stress is 168.06 MPa, which is less than the allowable value 306 MPa. Time history of equivalent strain and stress at node B are shown in Fig. 38 and Fig. 39, respectively, the equivalent strain and stress increase with time, but the value is very small.

For Case 3, at the last step at the last step 7.1929×10^{-3} sec, the stress intensity distribution and equivalent strain are shown in Fig. 40 and Fig. 41, respectively, the maximum equivalent strain is 0.0277%, which is less than the allowable value 11%. The membrane

stress and membrane plus bending stress along path 4 is plotted in Fig. 43, the maximum membrane stress is 36.21 MPa and is less than the allowable value 204 MPa; the maximum plus bending stress is 51.38 MPa and is also much less than the allowable value 306 MPa. Time history of equivalent strain and stress at node C are shown in Fig. 44 and Fig. 45, respectively, the equivalent strain and stress increase with time, but the value is very small.

Table 4 Summary of 2-D modeling structural analysis results

	Cases	Membrane stress (MPa)		Membrane plus bending stress (MPa)		Equivalent strain (%)	
		Calculated	Allowable Sm	Calculated	Allowable 1.5Sm	Calculated	Allowable
Static analysis	Design condition	123.83	204	171.61	306	0.0997	11
Transient analysis	CASE 1	126.99		145.66			
	CASE 2	140.05		168.06			
	CASE 3	36.21	51.38				

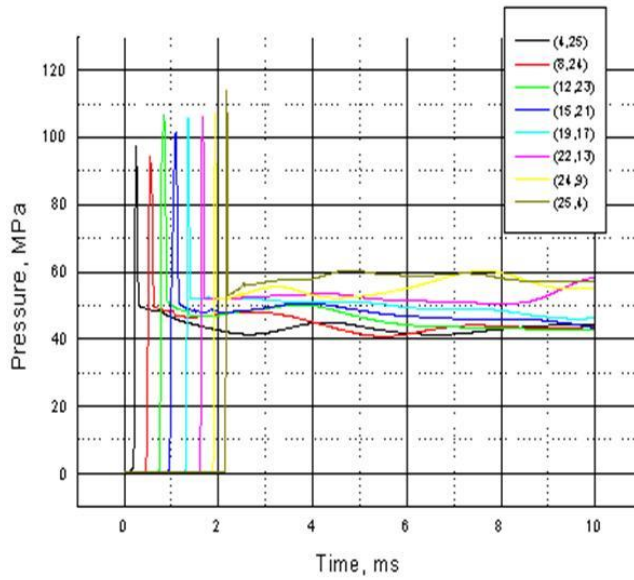


Fig. 15 Time history of explosion pressure in case of starting explosion at the bottom of the head

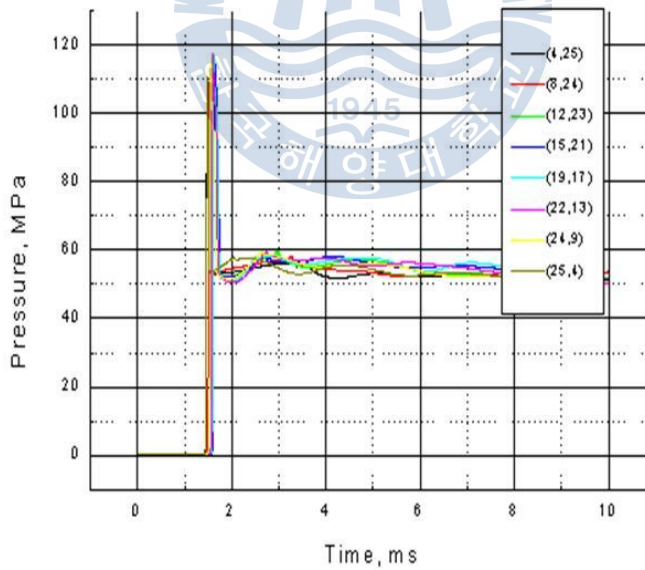


Fig. 16 Time history of explosion pressure in case of starting explosion at the top of the head

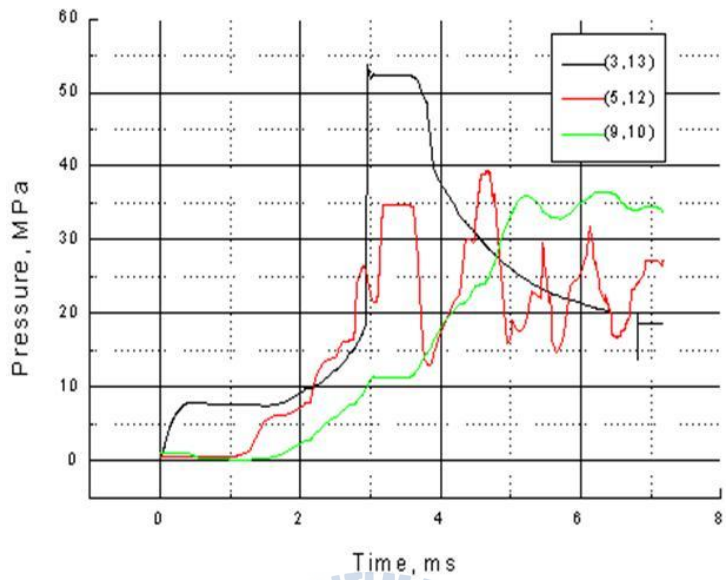
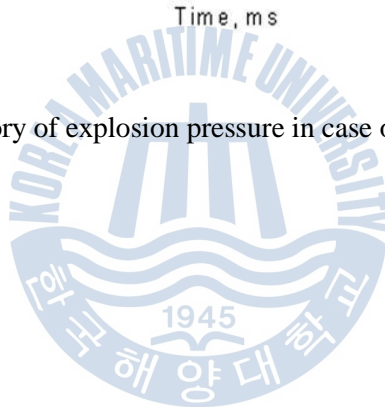


Fig. 17 Time history of explosion pressure in case of single jet mixing



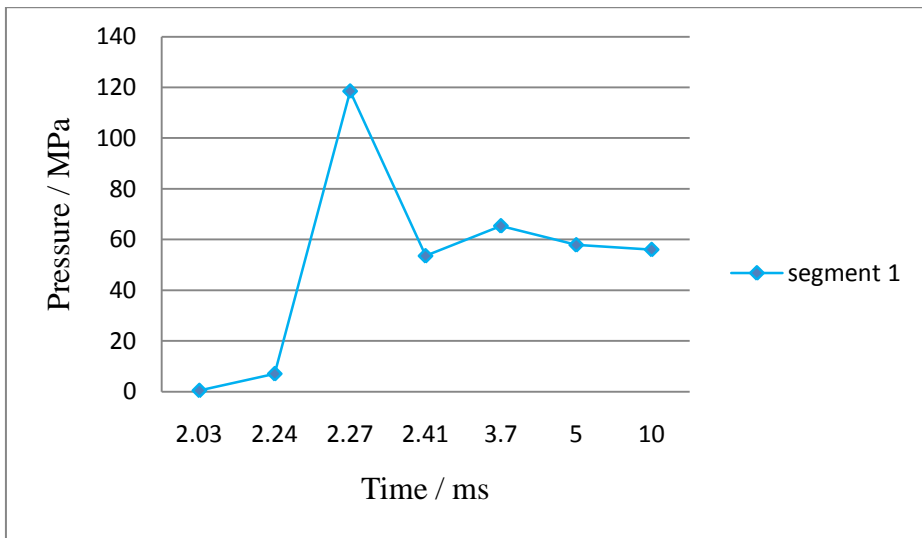


Fig. 18 Input time history of explosion pressure applied on 7 segments of inside of the head (CASE 1)

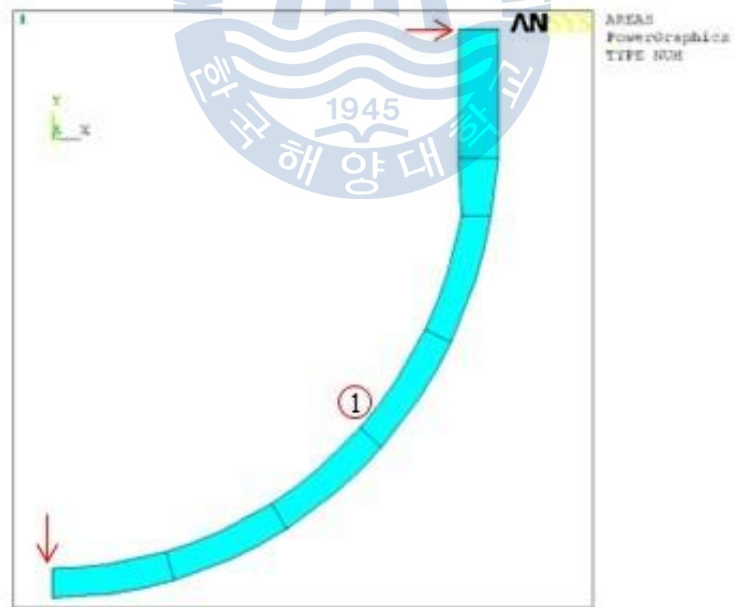


Fig. 19 Pressure loaded locations of lower head for CASE 1

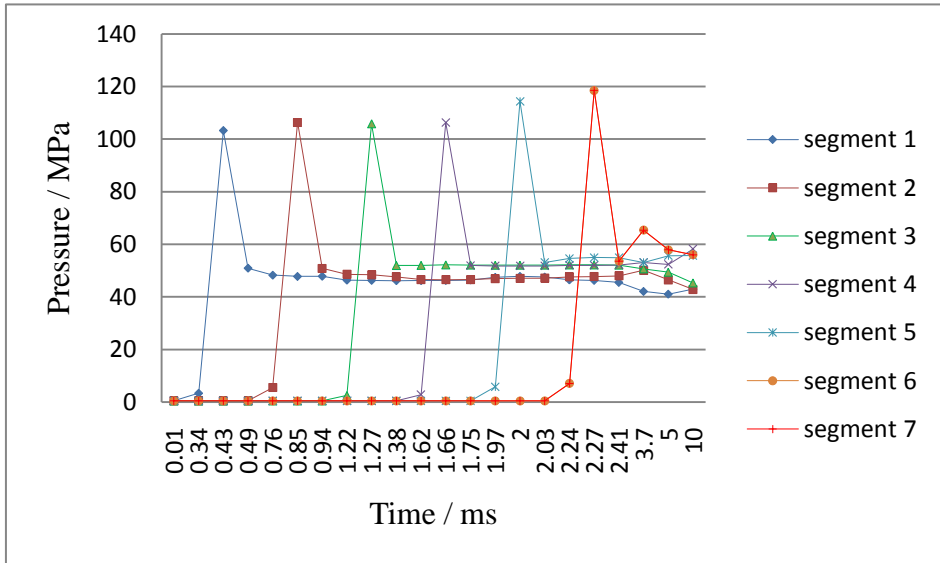


Fig. 20 Input time history of explosion pressure applied on 7 segments of inside of the head (CASE 2)

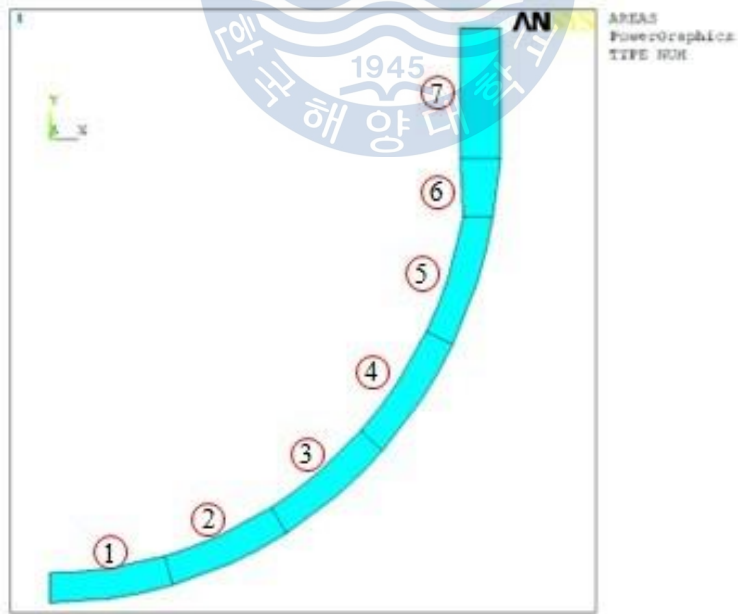


Fig. 21 Pressure loaded locations of lower head for CASE 2

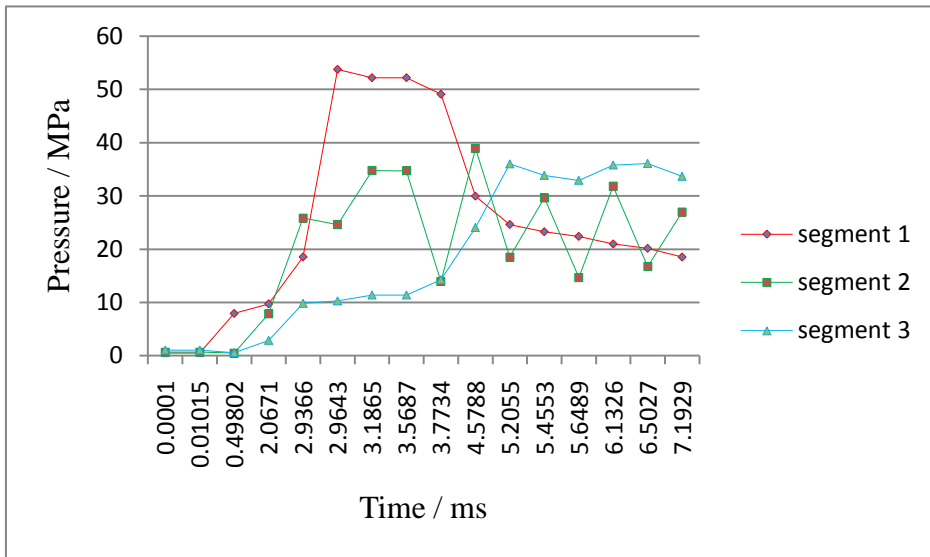


Fig. 22 Input time history of explosion pressure applied uniformly in case of single jet mixing (CASE 3).

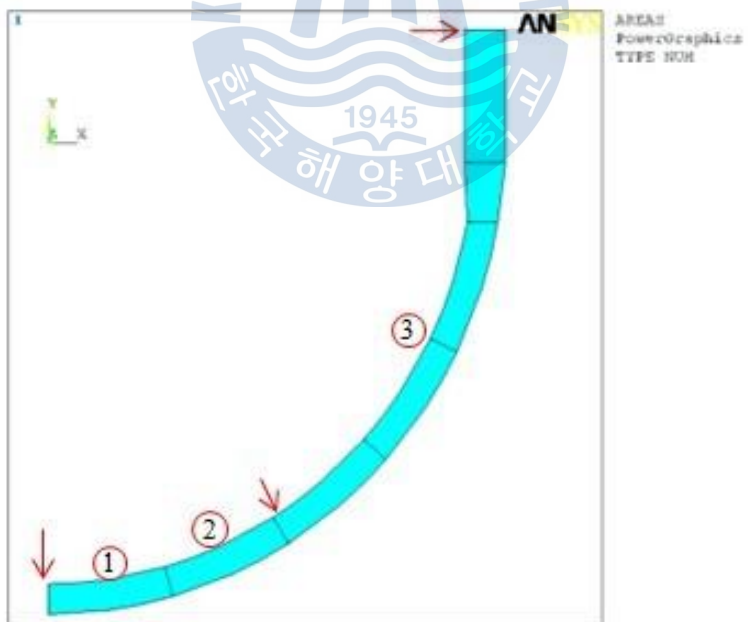


Fig. 23 Pressure loaded locations of lower head for CASE 3

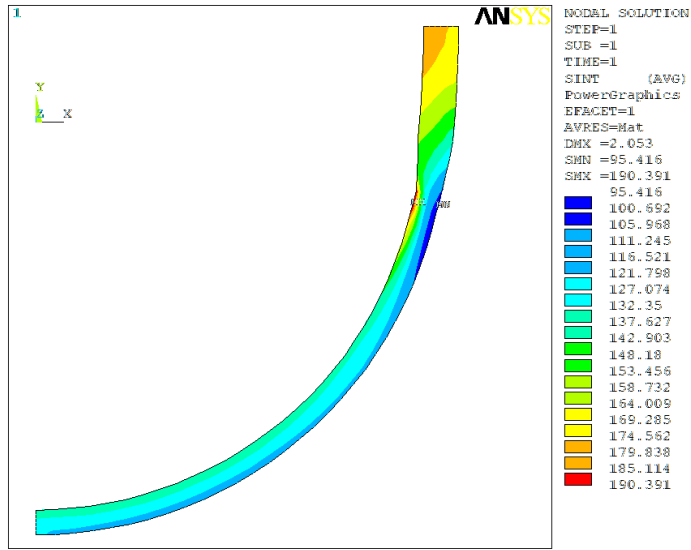


Fig. 24 Stress intensity distribution of 2-D model structural analysis under design condition

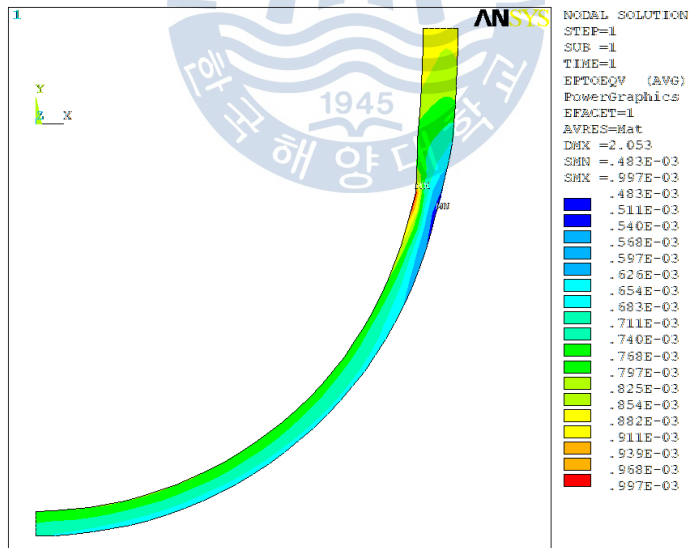


Fig. 25 Equivalent strain distribution of 2-D model structural analysis under design condition

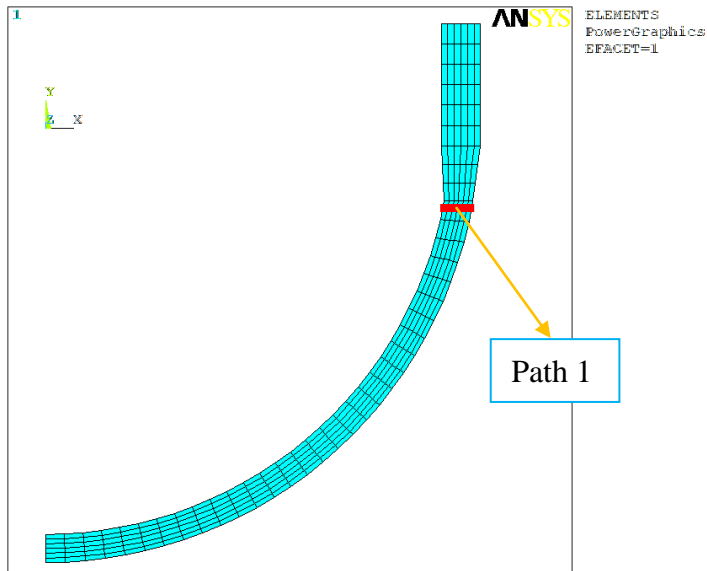


Fig. 26 Path 1 of 2-D model structural analysis under design condition

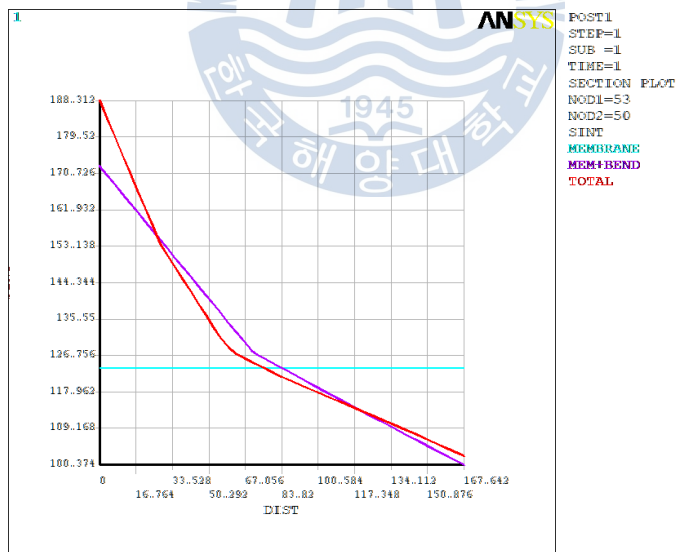


Fig. 27 Membrane and membrane plus bending stress along Path 1 of 2-D model structural analysis under design condition

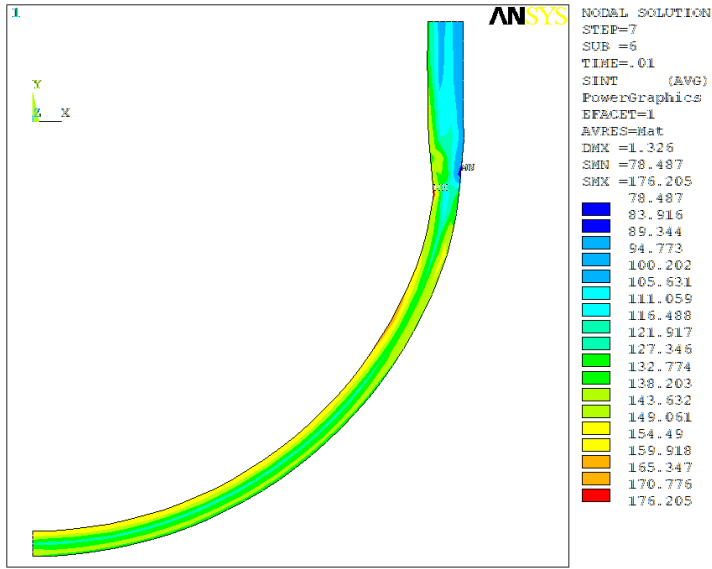


Fig. 28 Stress intensity distribution at 0.01 sec of 2-D model structural analysis for CASE1

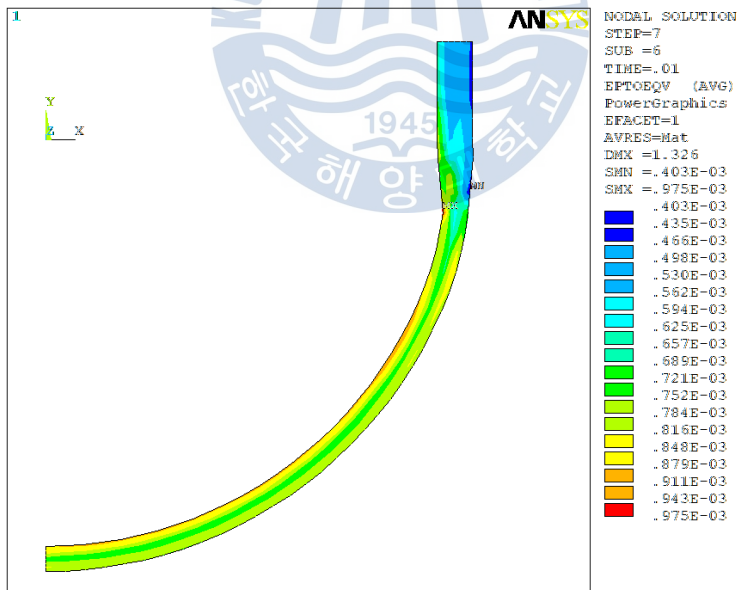


Fig. 29 Equivalent strain distribution at 0.01 sec of 2-D model structural analysis for

CASE 1

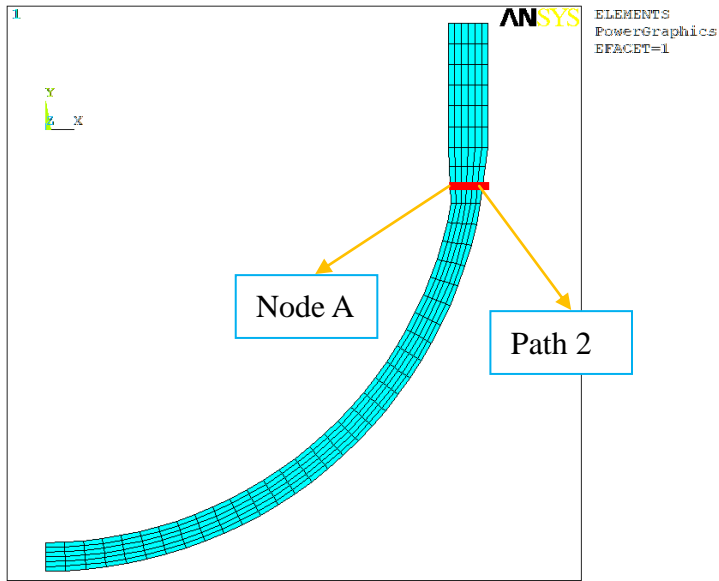


Fig. 30 Path 1 and Node A of 2-D model structural analysis for CASE 1

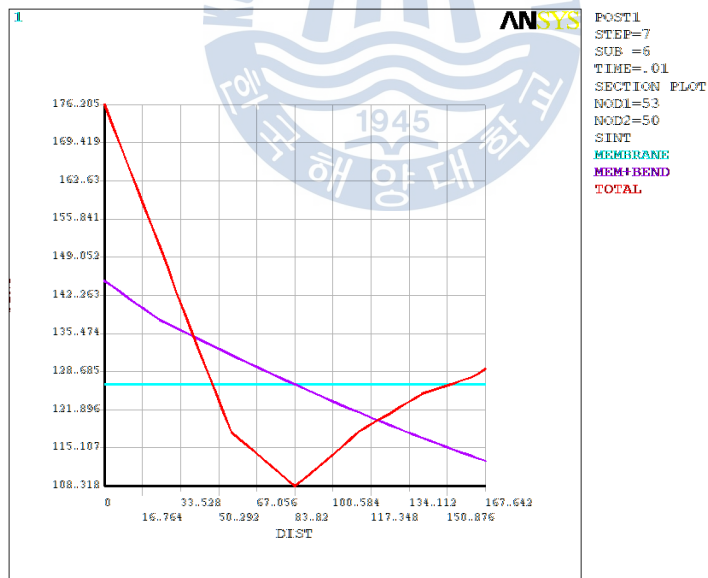


Fig. 31 Membrane and membrane plus bending stress at 0.01 sec along Path 2 of 2-D model structural analysis for CASE 1

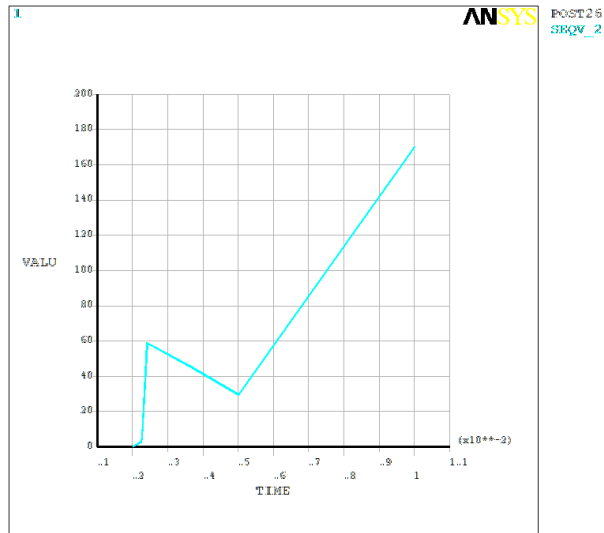


Fig. 32 Time history of equivalent stress at Node A of 2-D model structural analysis for

CASE 1

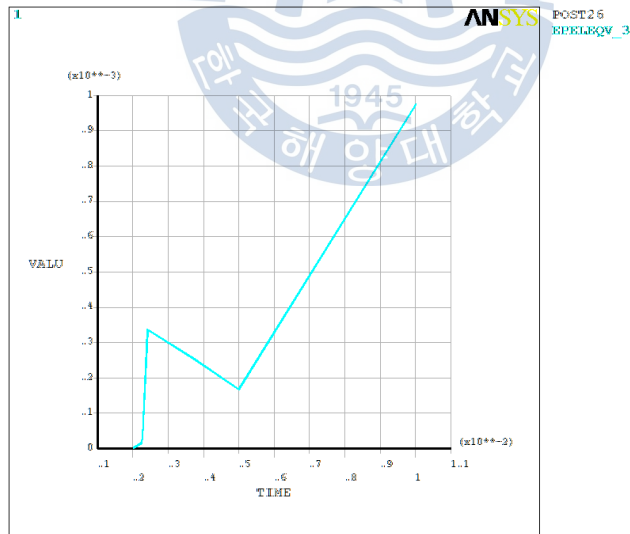


Fig. 33 Time history of equivalent strain at Node A of 2-D model structural analysis for

CASE 1

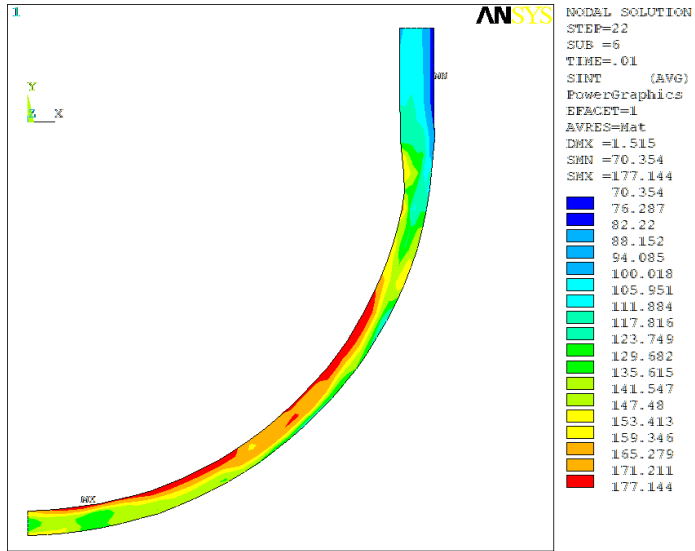


Fig. 34 Stress intensity distribution at 0.01 sec of 2-D model structural analysis for CASE2

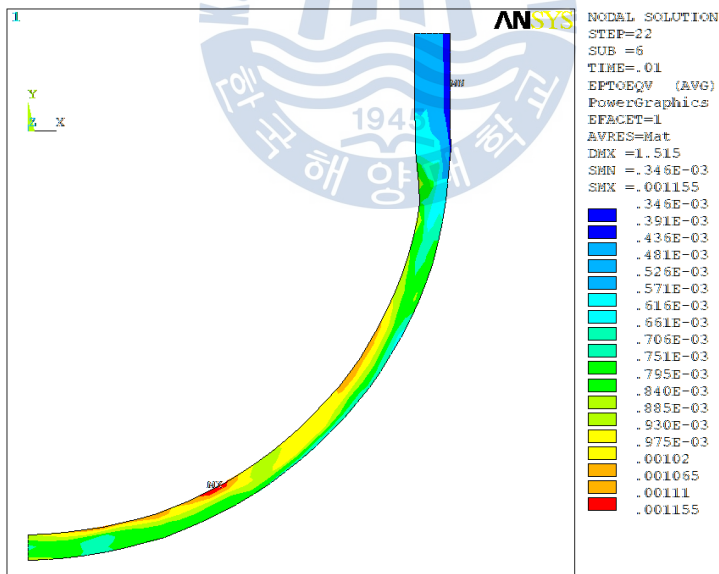


Fig. 35 Equivalent strain distribution at 0.01 sec of 2-D model structural analysis for

CASE 2

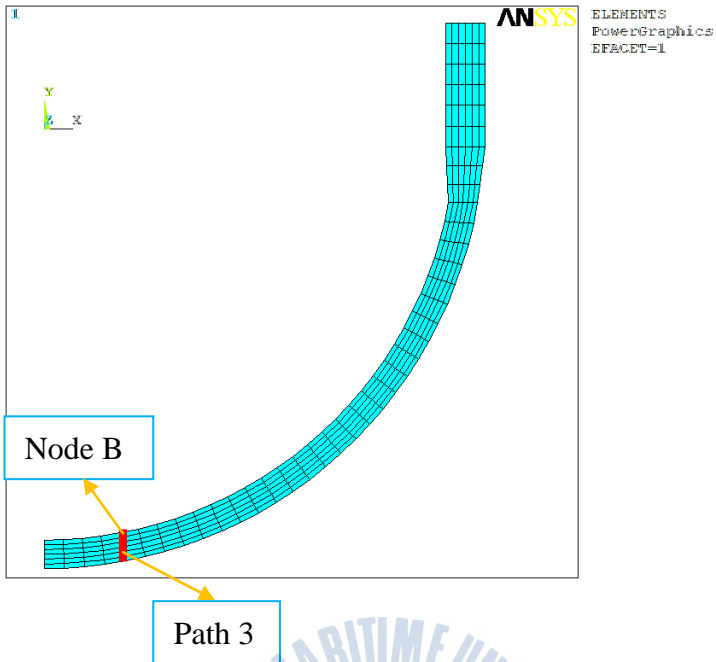


Fig. 36 Path 1 and Node A of 2-D model structural analysis for CASE 2

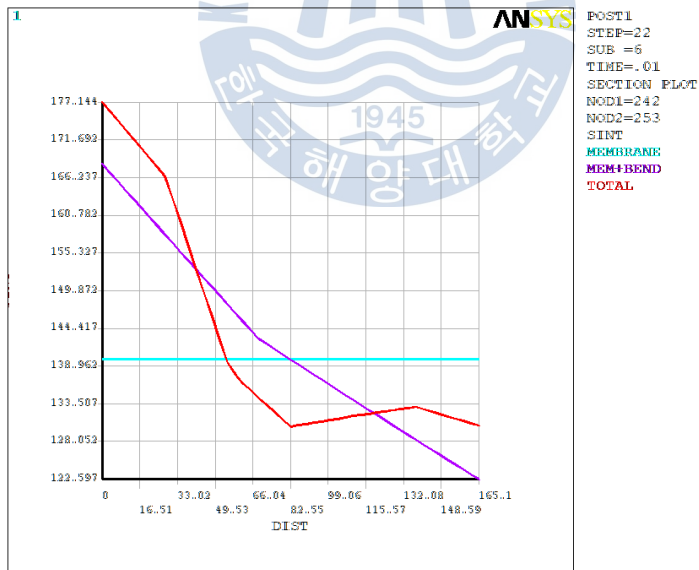


Fig. 37 Membrane and membrane plus bending stress at 0.01 sec along Path 3 of 2-D model structural analysis for CASE 2

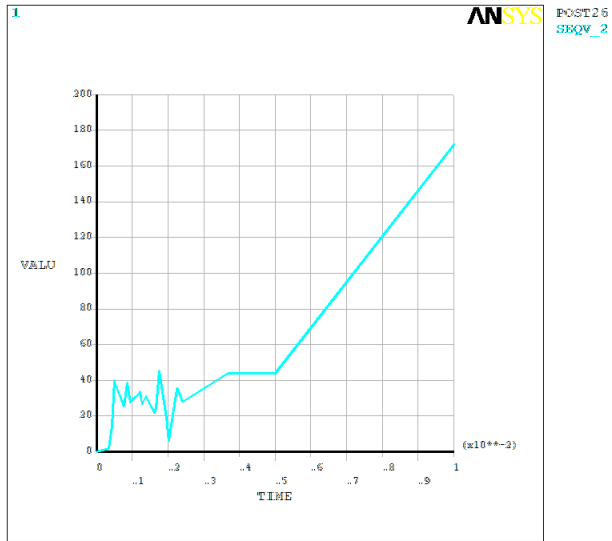


Fig. 38 Time history of equivalent stress at Node B of 2-D model structural analysis for

CASE 2

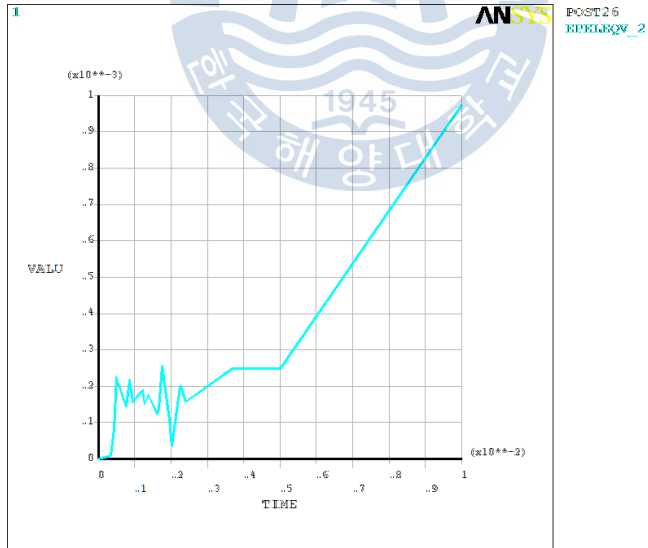


Fig. 39 Time history of equivalent strain at Node B of 2-D model structural analysis for

CASE 2

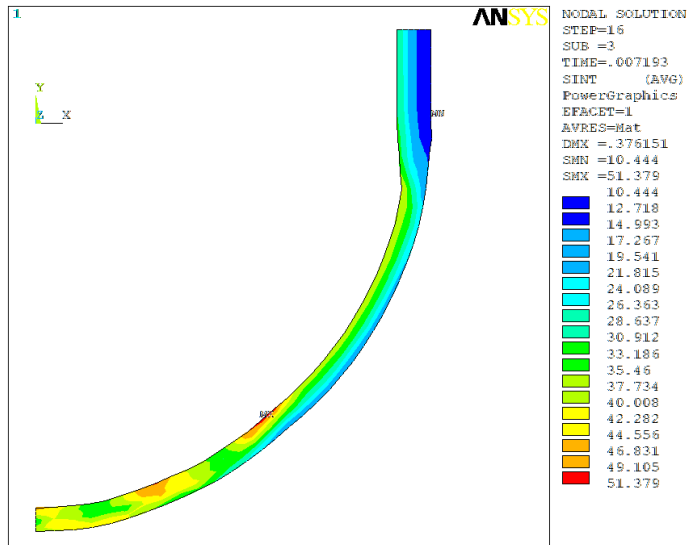


Fig. 40 Stress intensity distribution at 0.0072 sec of 2-D model structural analysis for

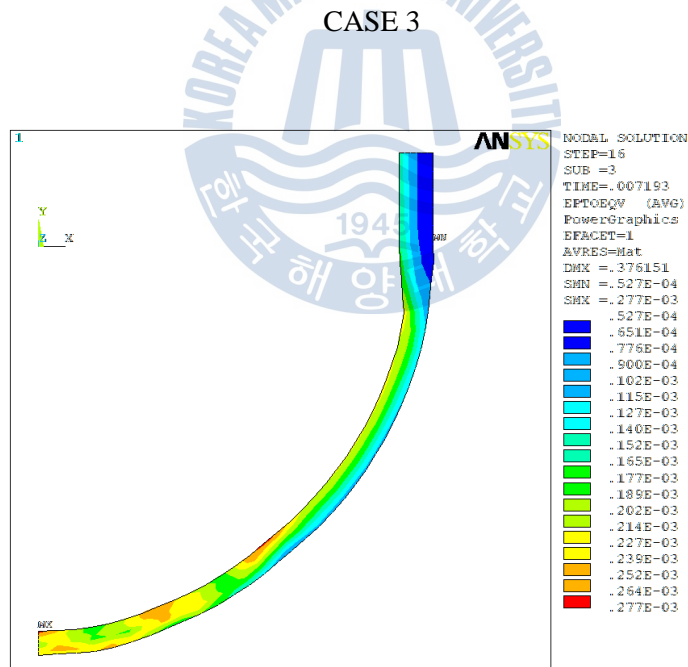


Fig. 41 Equivalent strain distribution at 0.0072 sec of 2-D model structural analysis for

CASE 3

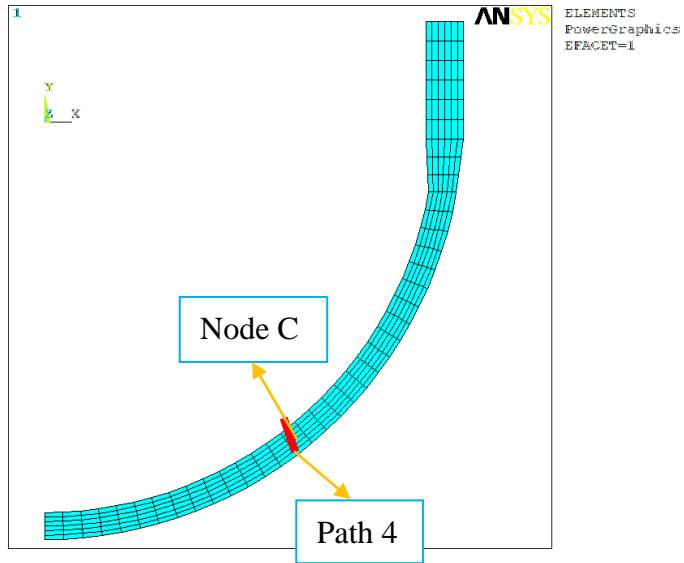


Fig. 42 Path 1 and Node A of 2-D model structural analysis for CASE 3

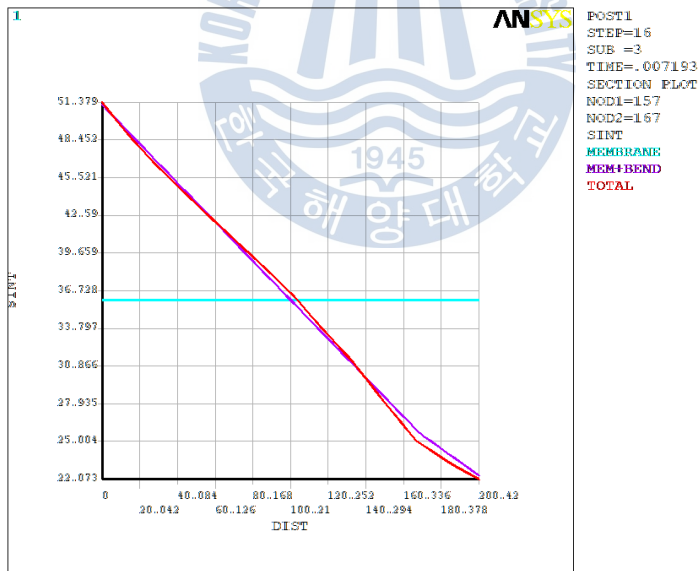


Fig. 43 Membrane and membrane plus bending stress at 0.0072 sec along Path 4 of 2-D model structural analysis for CASE 3

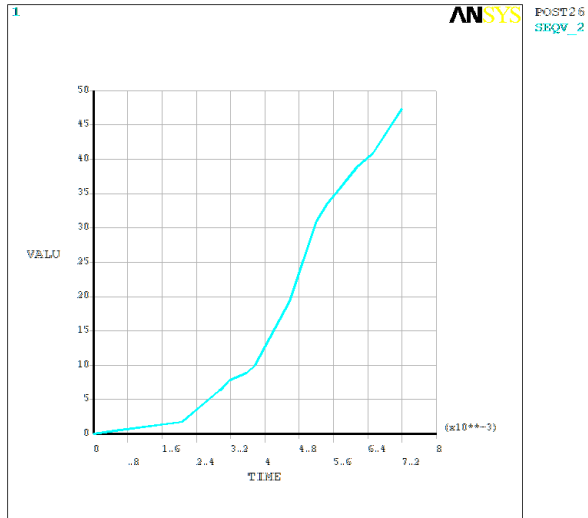


Fig. 44 Time history of equivalent stress at Node C of 2-D model structural analysis for

CASE 3

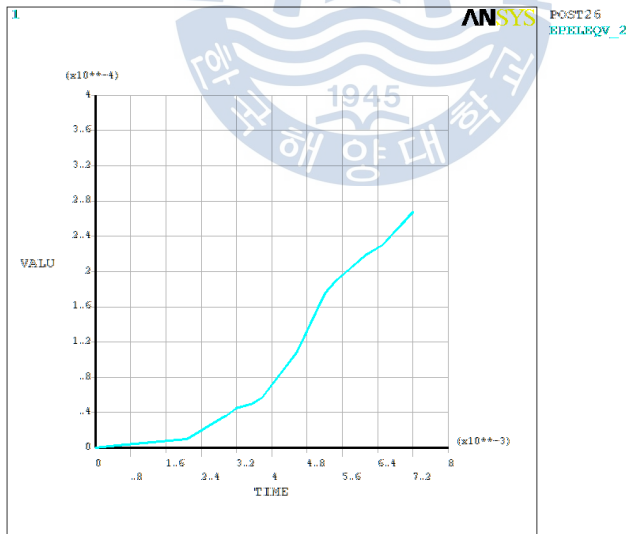


Fig. 45 Time history of equivalent strain at Node C of 2-D model structural analysis for

CASE 3

3.2 Structural analysis of 3-D model lower head

For 3-D model analysis, all the loading pressure values and material properties are as same as 2-D situation, the only different thing is that the pressure applies not only on the inside surface of lower head but also on the top surface and side surface of three pipes.

3.2.1 Stress analysis under design condition

The pressure of design condition is 17.24 MPa, which is applied on the inner side of the head, the side surfaces and top surface of 3 pipes.

3.2.2 Transient dynamic analysis of explosion load

Three CASES transient dynamic pressures apply on the inner side of the head, side surfaces and top surface of 3 pipes. The pressure values are shown in Fig. 18, Fig. 20 and Fig. 22, respectively.

3.2.3 Results of 3-D modeling structural analysis

There are two situations: results under design condition and transient dynamic explosion loads.

3.2.3.1 Stress analysis results under design condition

A contour plot of the stress intensity is shown in Fig. 46, the maximum stress intensity is 235.79 MPa at connection between the lower head and the second pipe. A plot of sections stresses across the wall thickness of a section is shown in Fig 49, the maximum membrane stress intensity is 176.23 MPa, which is less than the allowable value of 204 MPa; the

maximum membrane plus bending stress intensity is 203.58 MPa, which is less than the allowable value of 306 MPa. The equivalent strain distribution is shown in Fig.47, the maximum equivalent strain is 0.3223% and is much less than the allowable value of 11%.

3.2.3.2 Transient dynamic analysis of explosion load results

For CASE 1, at the last step 0.01 sec, the stress intensity distribution and equivalent strain distribution are shown in Fig. 50 and Fig. 51, respectively, the maximum equivalent strain is 0.3084%, which much less than the allowable value 11%. The membrane stress and membrane plus bending stress along path 6 is plotted in Fig. 50, the maximum membrane stress is 189.63 MPa and is less than the allowable value 204 MPa; the maximum membrane plus bending stress is 237.07 MPa and is less than the allowable value 306 MPa. Time history of equivalent strain and stress at node D are shown in Fig. 54 and Fig. 52, respectively, both the value increase with time, but the value is very small.

For CASE 2, at the last step 0.01 sec, the stress intensity distribution and equivalent strain distribution are plotted in Fig. 56 and Fig. 57, respectively, the maximum equivalent strain is 0.3853% and is less than the allowable value 11%. The membrane stress and membrane plus bending stress along path 7 is plotted in Fig. 59, the maximum membrane stress is 199.07 MPa, which is less than the allowable value 204 MPa; the maximum membrane plus bending stress is 225.52 MPa, which is less than the allowable value 306 MPa. Time history of equivalent strain and stress at node E are shown in Fig. 60 and Fig. 61, respectively, the equivalent strain and stress increase with time, but the value is very small.

For CASE 3, at the last step at the last step 7.1929×10^{-3} sec, the stress intensity distribution and equivalent strain are shown in Fig. 62 and Fig. 63, respectively, the maximum equivalent strain is 0.1352%, which is less than the allowable value 11%. The

membrane stress and membrane plus bending stress along path 8 is plotted in Fig. 65, the maximum membrane stress is 46.91 MPa and is less than the allowable value 204 MPa; the maximum plus bending stress is 111.67 MPa and is also much less than the allowable value 306 MPa. Time history of equivalent strain and stress at node F are shown in Fig. 66 and Fig. 67, respectively, the equivalent strain and stress increase with time, but the value is very small.

Table 5 Summary results of 3-D modeling structural analysis

	Cases	Membrane stress (MPa)		Membrane plus bending stress (MPa)		Equivalent strain (%)	
		Calculated	Allowable Sm	Calculated	Allowable 1.5Sm	Calculated	Allowable
Static analysis	Design condition	176.23	204	203.58	306	0.3223	11
Transient analysis	CASE 1	189.63		237.07			
	CASE 2	199.07		225.52			
	CASE 3	46.91	111.67				

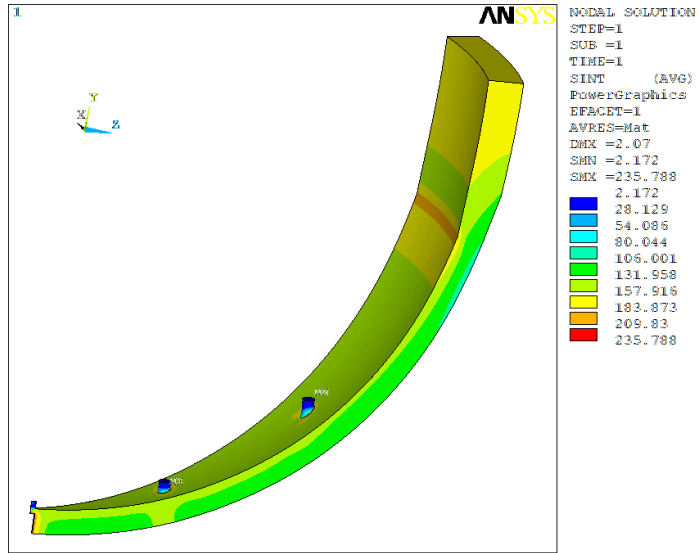


Fig. 46 Stress intensity distribution of 3-D model structural analysis under design condition

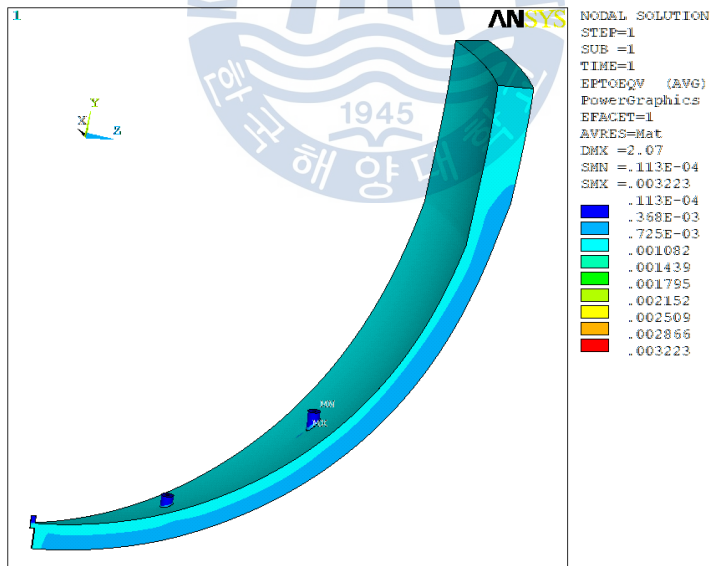


Fig. 47 Equivalent strain distribution of 3-D model structural analysis under design condition

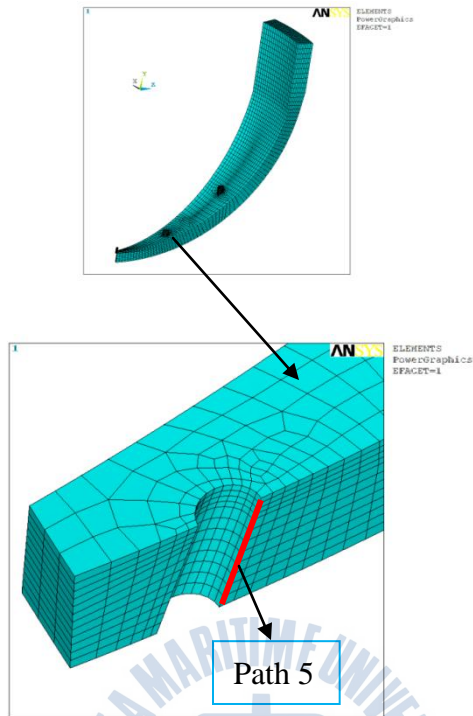


Fig. 48 Path 1 of 3-D model structural analysis under design condition

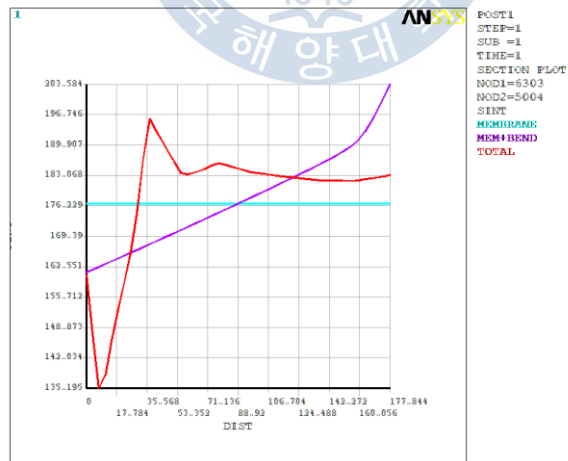


Fig. 49 Membrane and membrane plus bending stress along Path 5 of 3-D model structural analysis under design condition

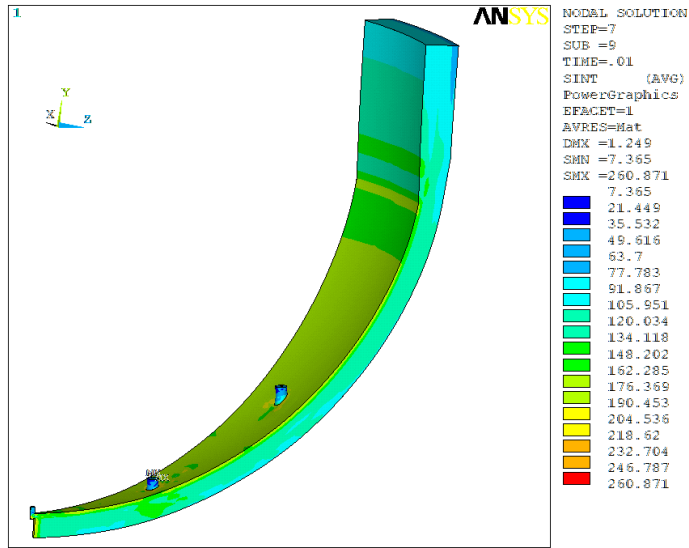


Fig. 50 Stress intensity distribution at 0.01 sec of 3-D model structural analysis
 for CASE 1

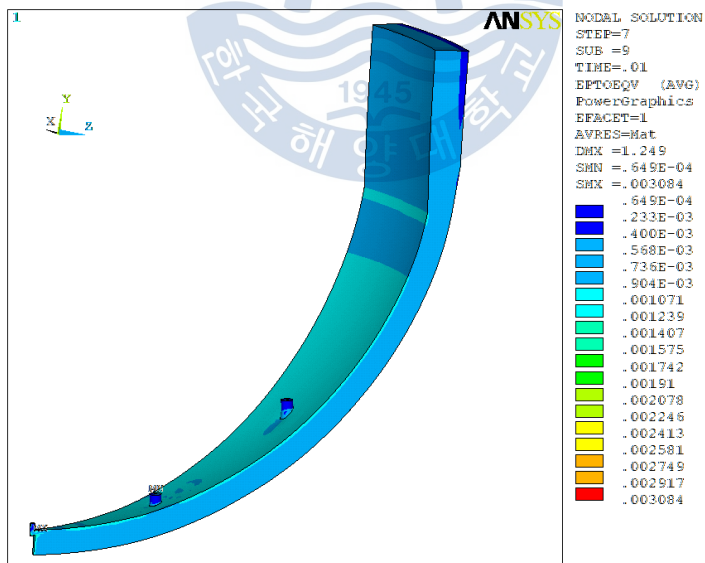


Fig. 51 Equivalent strain at 0.01 sec of 3-D model structural analysis
 for CASE 1

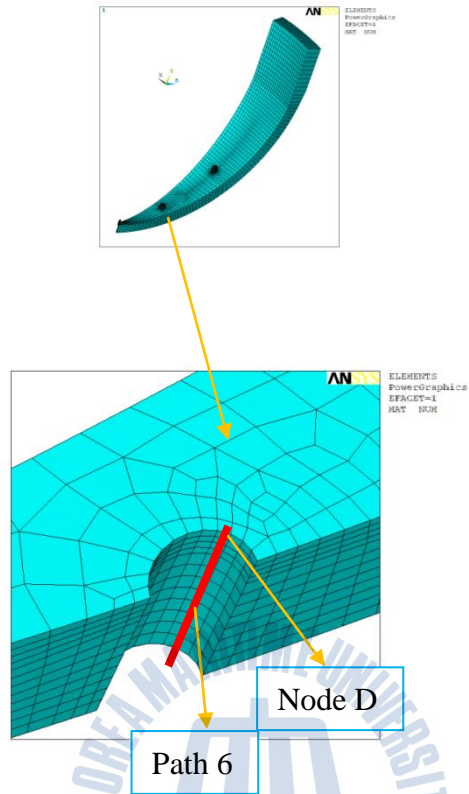


Fig. 52 Path 1 and Node A of 3-D model structural analysis for CASE 1

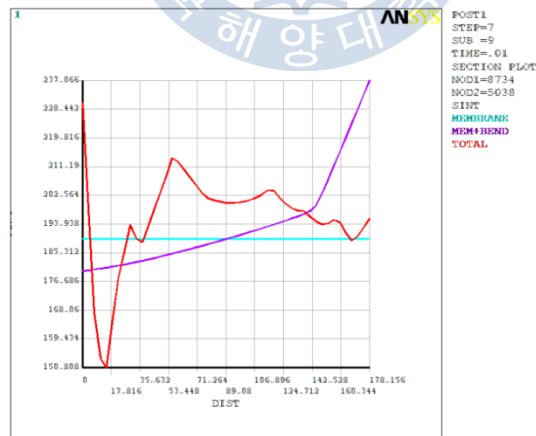


Fig. 53 Membrane and membrane plus bending stress at 0.01 sec along Path 6 of 3-D model structural analysis for CASE 1

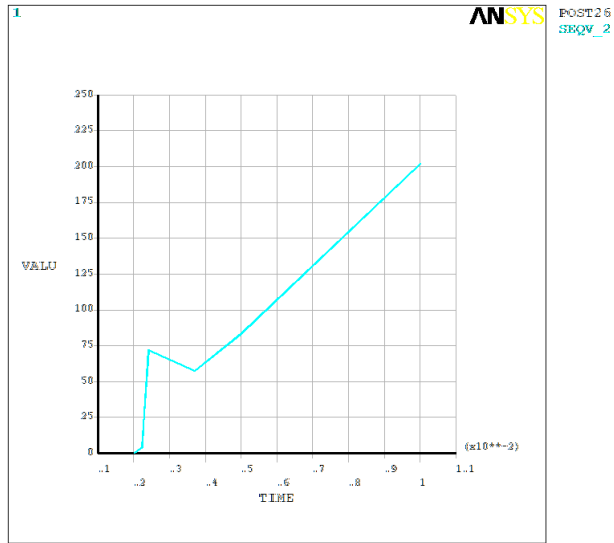


Fig. 54 Time history of equivalent stress at Node D of 3-D model structural analysis
for CASE 1

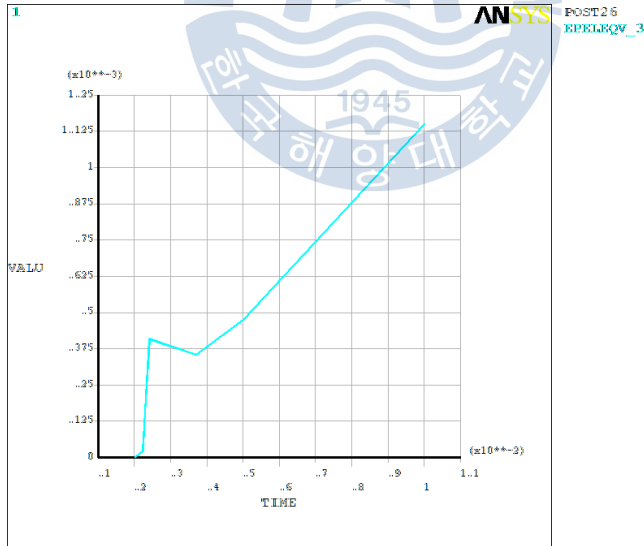


Fig. 55 Time history of equivalent strain at Node D of 3-D model structural analysis
for CASE 1

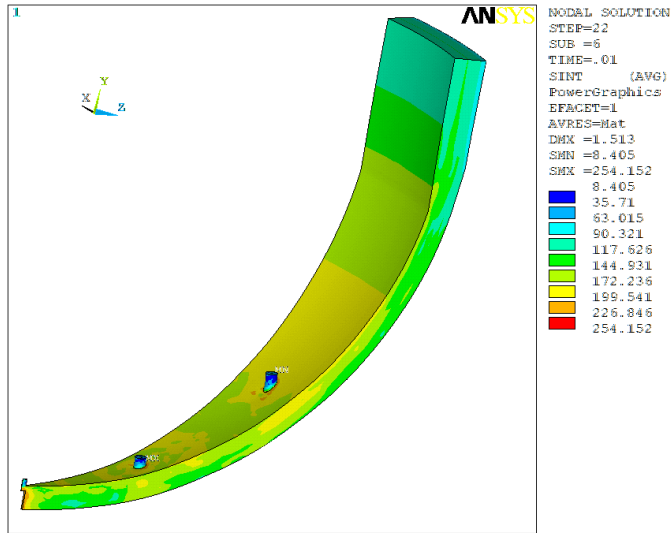


Fig. 56 Stress intensity distribution at 0.01 sec of 3-D model structural analysis
 for CASE 2

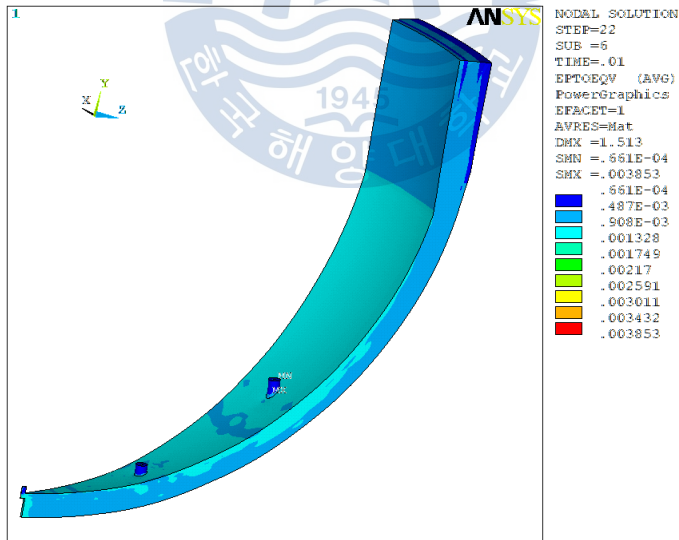


Fig. 57 Equivalent strain distribution at 0.01 sec of 3-D model structural analysis
 for CASE 2

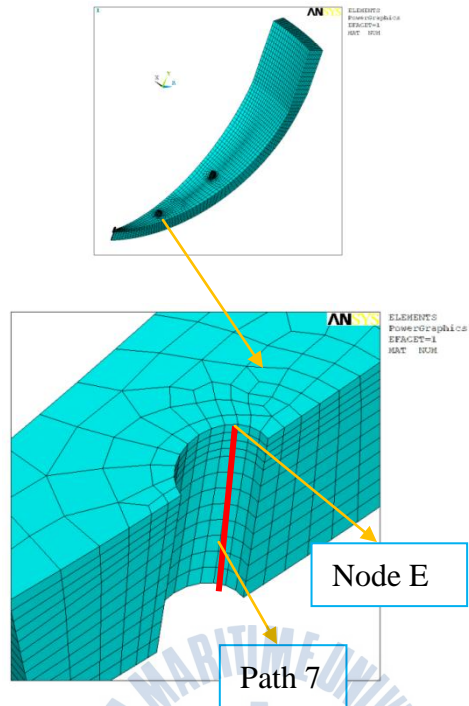


Fig. 58 Path 1 and Node A of 3-D model structural analysis for CASE 2

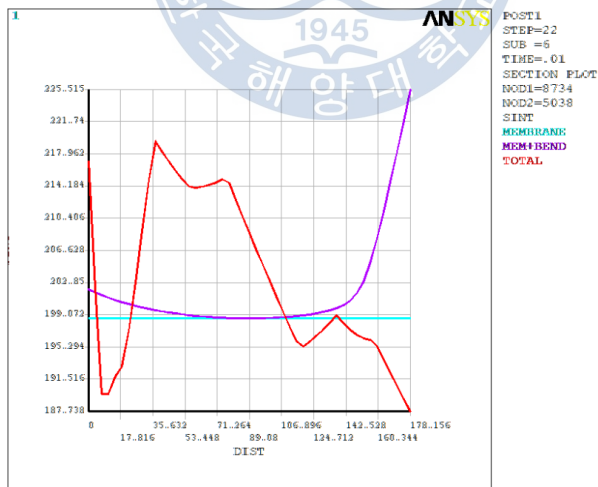


Fig. 59 Membrane and membrane plus bending stress at 0.01 sec along Path 1 of 3-D model structural analysis for CASE 2

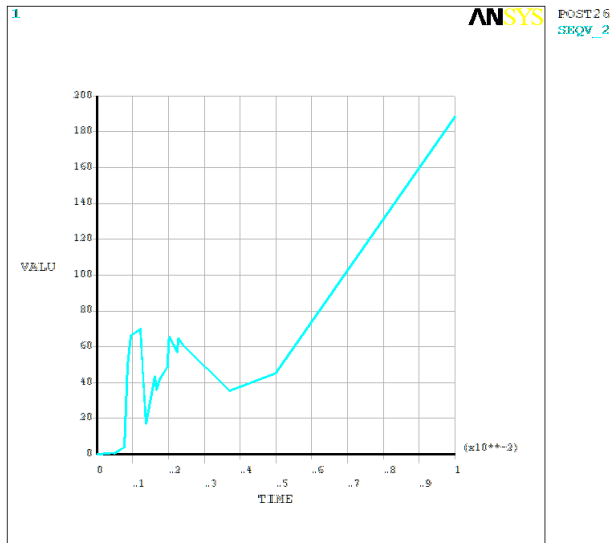


Fig. 60 Time history of equivalent stress at Node A of 3-D model structural analysis for

CASE 2

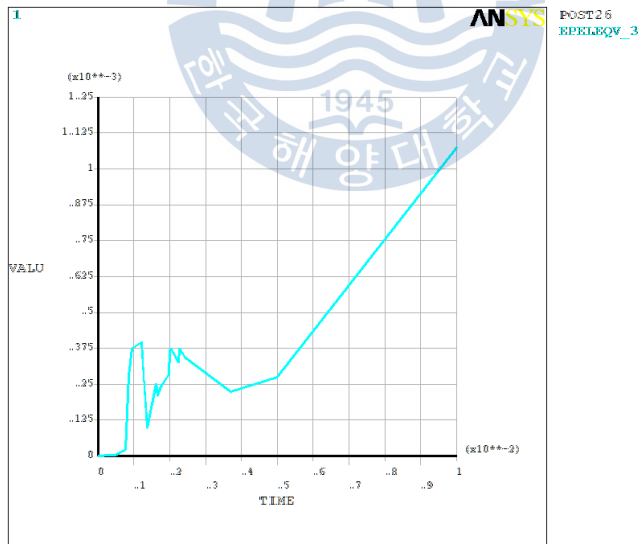


Fig. 61 Time history of equivalent strain at Node A of 3-D model structural analysis

for CASE 2

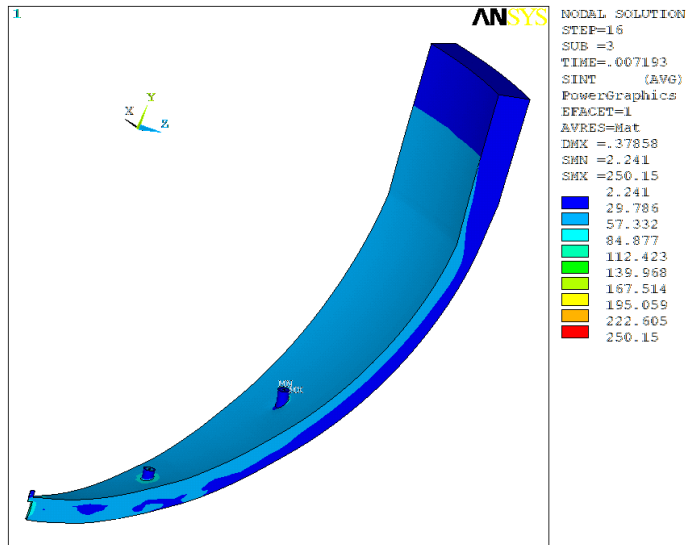


Fig. 62 Stress intensity distribution at 0.0072 sec of 3-D model structural analysis for

CASE 3

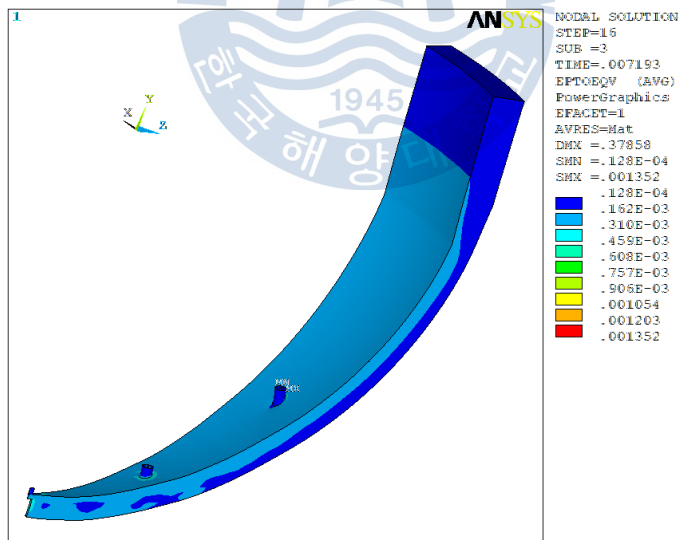


Fig. 63 Equivalent strain distribution at 0.0072 sec of 3-D model structural analysis for

CASE 3

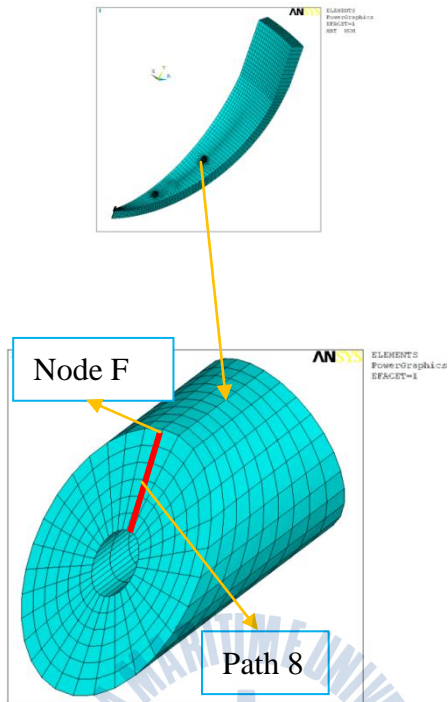


Fig. 64 Path 1 and Node A of 3-D model structural analysis for CASE 3

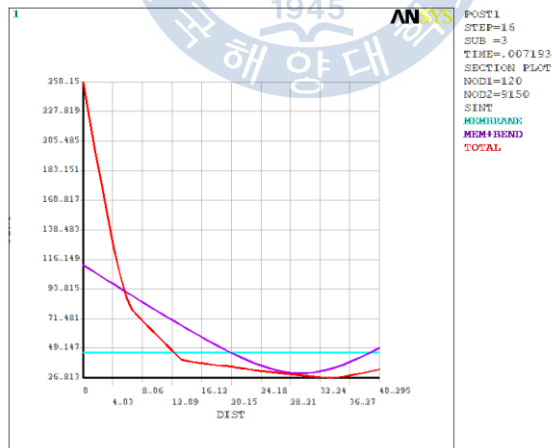


Fig. 65 Membrane and membrane plus bending stress at 0.0072 sec along Path 8 of 3-D model structural analysis for CASE 3

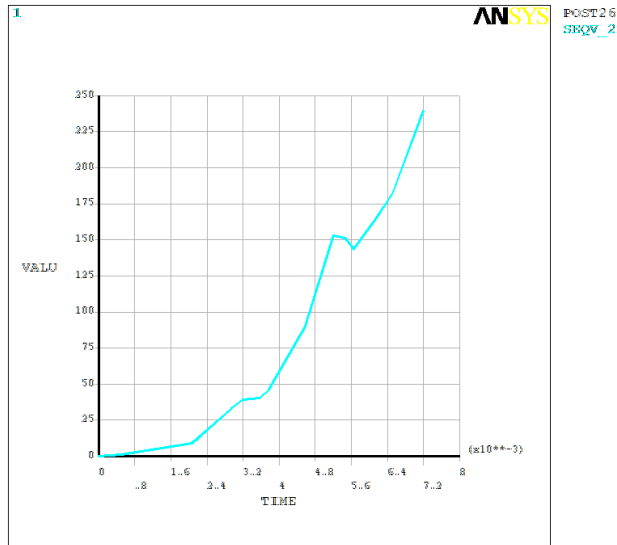


Fig. 66 Time history of equivalent strain at Node F of 3-D model structural analysis for

CASE 3

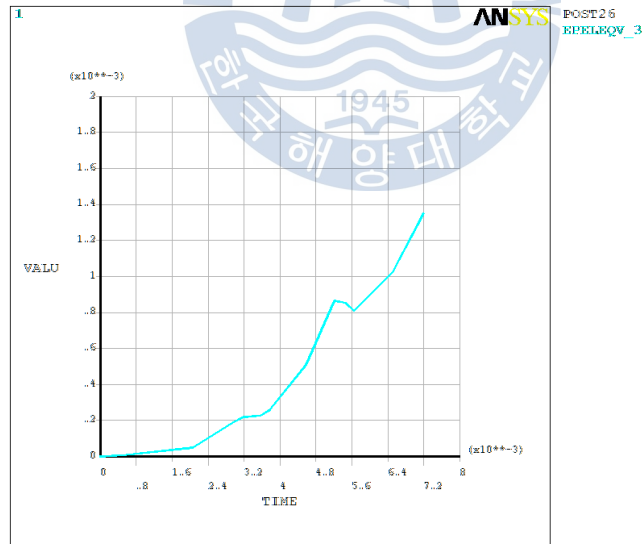


Fig. 67 Time history of equivalent strain at Node F of 3-D model structural analysis for

CASE 3

3.3 Thermal Analysis

The thermal analysis process is: using the calculated explosion temperature imposed on the lower head inside wall and the convection boundary condition imposed on the lower head outside wall, temperature distribution and heat flux calculation are performed by ANSYS program, then comparing the calculated heat flux value with the allowable boiling failure criteria heat flux value to determine the boiling failure.

3.3.1 Introduction

According to the experiment results[6], the vessel wall experiences the temperature field maintained by the convection varying from 400°C to 700°C along the polar angle.

The lower head is quenched down to saturation water at 100°C and 0.1Mpa .

3.3.2 Loading data

Table 6 Loading data for thermal analysis

Inside	Segment	1	2	3	4	5	6	7
Surface	Temperature (°C)	400	460	520	580	640	700	260
Outside	Temperature: 100°C							
Surface	Convection Heat Transfer Coefficient: 30000W/ m ² . °C							

Table 7 Material mechanical proprieties of thermal analysis

Properties	Temperature (°C)							
	100	260	400	460	520	580	640	700
Young's modulus (GPa)	187	177.2	167	162	156	149.4	142.2	133
Poisson's ratio	0.308	0.312	0.312	0.314	0.317	0.320	0.323	0.326
Thermal expansion coefficient $\times 10^{-6}(\text{m}/\text{m}/\text{°C})$	6.72	7.3	7.7	7.9	8.05	8.15	8.3	8.4
Thermal conduction (W / m. °C)	40.6	39.3	36.8	35.55	34.5	33.1	31.8	29.1
Yield Strength (MPa)	453	422	397	373	336	336	336	336
Density (kg / m ³)	8110	8110	8110	8110	8110	8110	8110	8110

3.3.3 Thermal analysis results

The temperature distribution of lower head is shown in Fig. 68. The heat flux distribution is shown in Fig. 69, the maximum heat flux is 167.67 kW/ m², which is less than the allowable value 500 kW/ m², so it will not occur boiling crisis.

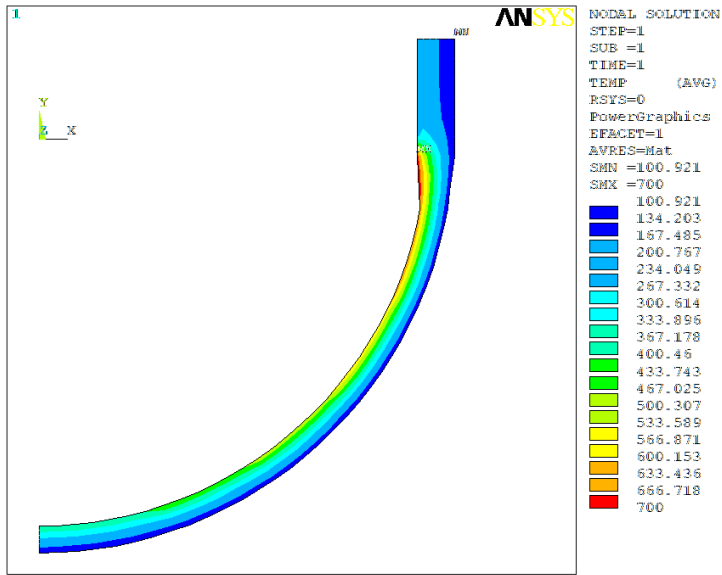


Fig. 68 Temperature distribution of 2-D model of lower head

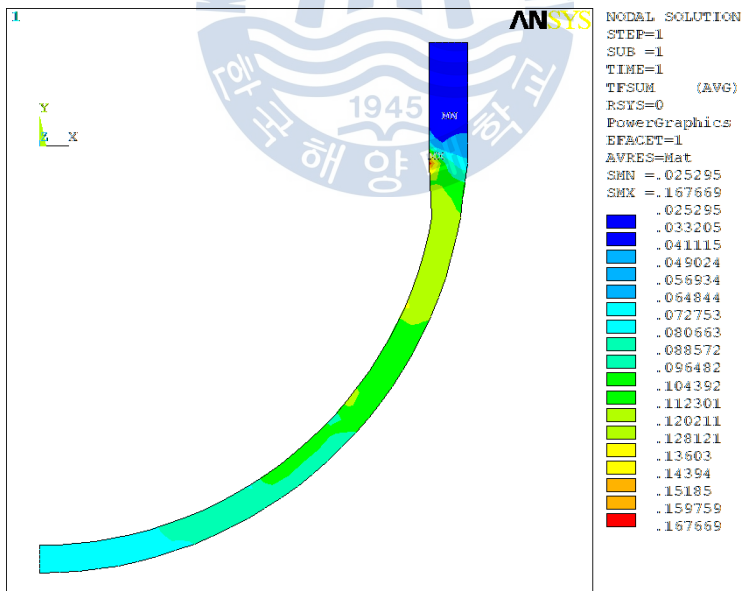


Fig. 69 Thermal flux distribution of 2-D model of lower head

3.4 Thermo-mechanical analysis for 2-D modeling

For this process, both the calculated explosion pressure and the thermal analysis result are applied on the lower head inner wall, total strain (total mechanical and thermal strain) and stress calculation are performed by ANSYS program, then compare the calculated value with the allowable failure criteria value to determine the failure of the lower head.

3.4.1 Thermo-mechanical analysis under design condition

The pressure of design condition is 17.24 MPa, which is applied on the inner side of the head.

Table 8 Loading data for thermo-mechanical analysis under design condition

Loadings	Data
Thermal load	Temperature from heat transfer analysis as shown in Fig. 68
Pressure load	17.24 (MPa)
Reference temperature	30 °C

The material mechanical properties for the thermo-mechanical analysis are as same as the thermal analysis values, which are listed in Table 7.

3.4.2 Thermo-mechanical analysis under transient dynamic of explosion load

The pressure application situation of thermo-mechanical analysis is as same as the structural analysis situation.

Table 9 Loading data for thermo-mechanical analysis under transient explosion

Loadings	Data
Thermal load	Temperature from heat transfer analysis as shown in Fig. 68
Pressure load	As shown in Fig.18, Fig.20 and Fig.22
Reference temperature	30 °C

3.4.3 Results of thermo-mechanical analysis

There are two situations: results under design condition and transient dynamic explosion load.

3.4.3.1 Thermo-mechanical analysis results under design condition

A contour plot of the stress intensity is shown in Fig. 70, the maximum stress intensity is 233.39 MPa. A plot of sections stresses across the wall thickness of a section is shown in Fig 73, the maximum membrane stress intensity is 131.51 MPa, which is less than the allowable value of 197 MPa; the maximum membrane plus bending stress intensity is 292.11 MPa, which is less than the allowable value of 295.5 MPa. The total strain distribution is shown in Fig. 71, the maximum value is 0.8083%, which is less than the allowable value 6%.

3.4.3.2 Thermo-mechanical analysis results under transient dynamic of explosion load

For CASE 1, at the last step 0.01 sec, the stress intensity distribution and total strain distribution are shown in Fig. 74 and Fig. 75, respectively, the maximum value is 1.2603%, which is less than the allowable value 6%. The membrane stress and membrane plus bending stress along path 10 is plotted in Fig. 77, the maximum membrane stress is 166.33

MPa and is less than the allowable value 197 MPa; the maximum membrane plus bending stress is 208.50 MPa and is less than the allowable value 295.5 MPa. Time history of equivalent strain and stress at node G are shown in Fig. 78 and Fig. 79 respectively, both the value increase with time, but the value is very small.

For CASE 2, at the last step 0.01 sec, the stress intensity distribution and Total strain distribution are plotted in Fig. 80 and Fig. 81 respectively, the maximum value is 1.3237%, which is less than the allowable value 6%. The membrane stress and membrane plus bending stress along path 11 is plotted in Fig. 83, the maximum membrane stress is 190.09 MPa, which is less than the allowable value 197 MPa; the maximum membrane plus bending stress is 214.93 psi, which is less than the allowable value 295.5 MPa. Time history of equivalent strain and stress at node H are shown in Fig. 84 and Fig. 85 respectively, the equivalent strain and stress increase with time, but the value is very small.

For CASE 3, at the last step at the last step 7.1929×10^{-3} sec, the stress intensity distribution and total strain are shown in Fig. 86 and Fig. 87 respectively, the maximum value is 1.308%, which is less than the allowable value 6%. The membrane stress and membrane plus bending stress along path 12 is plotted in Fig. 89, the maximum membrane stress is 78.60 MPa and is less than the allowable value 197 MPa; the maximum plus bending stress is 161.76 MPa and is also much less than the allowable value 295.5 MPa. Time history of equivalent strain and stress at node I are shown in Fig. 90 and Fig. 91, respectively, the equivalent strain and stress increase with time, but the value is very small.

Table 10 Summary results of thermo-mechanical analysis

	CASES	Membrane stress (MPa)		Membrane plus bending stress (MPa)		Total strain (%)	
		Calculated	Allowable Sm	Calculated	Allowable 1.5Sm	Calculated	Allowable
Static analysis	Design condition	131.51	197	292.11	295.5	0.8083	6
Transient analysis	CASE1	166.33		208.50		1.2603	
	CASE 2	190.09		214.93		1.3237	
	CASE 3	78.60		161.76		1.308	



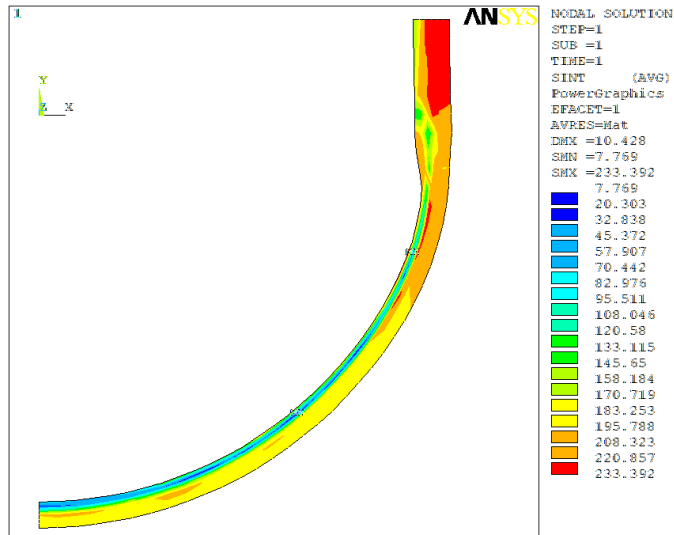


Fig. 70 Stress intensity distribution of 2-D model thermo-mechanical analysis under design condition

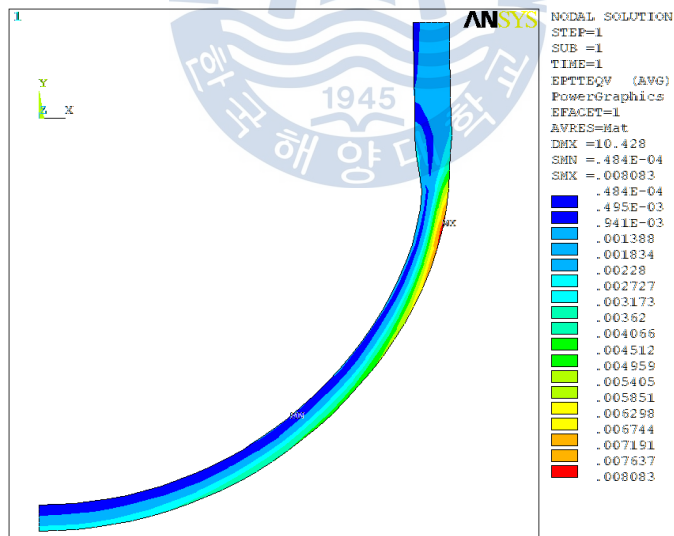


Fig. 71 Total strain distribution of 2-D model thermo-mechanical analysis under design condition

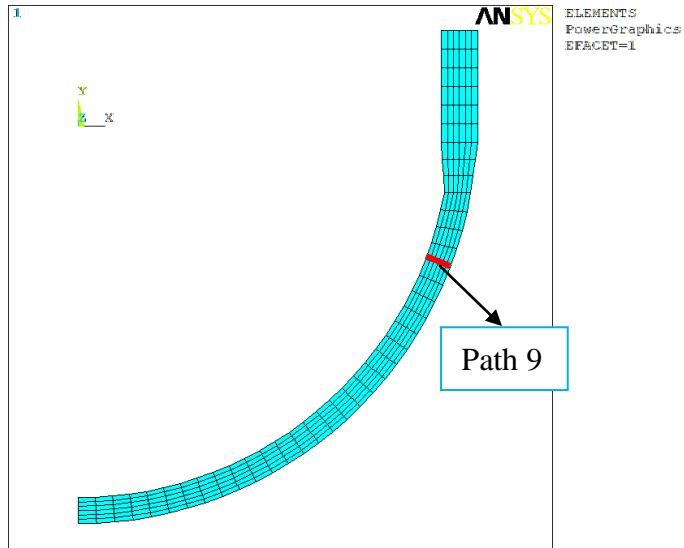


Fig. 72 Path 1 of 2-D model thermo-mechanical analysis under design condition

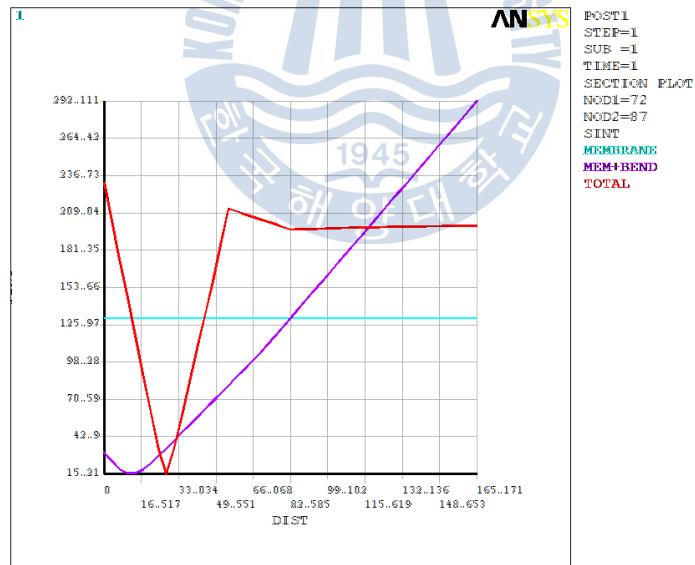


Fig. 73 Membrane and membrane plus bending stress along Path 9 of 2-D model thermo-mechanical analysis under design condition

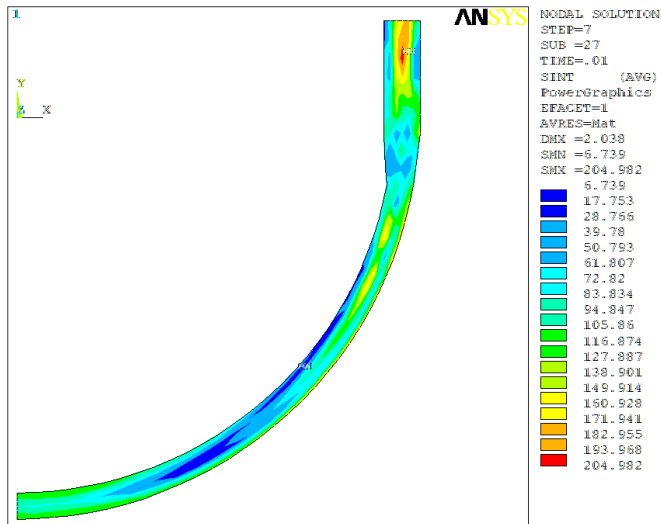


Fig. 74 Stress intensity distribution at 0.01 sec of 2-D model thermo-mechanical analysis
 for CASE 1

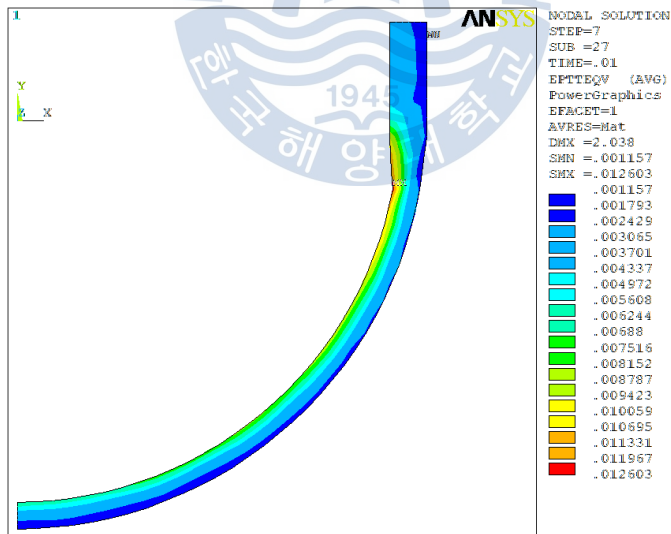


Fig. 75 Total strain distribution at 0.01 sec of 2-D model thermo-mechanical analysis for
 CASE 1

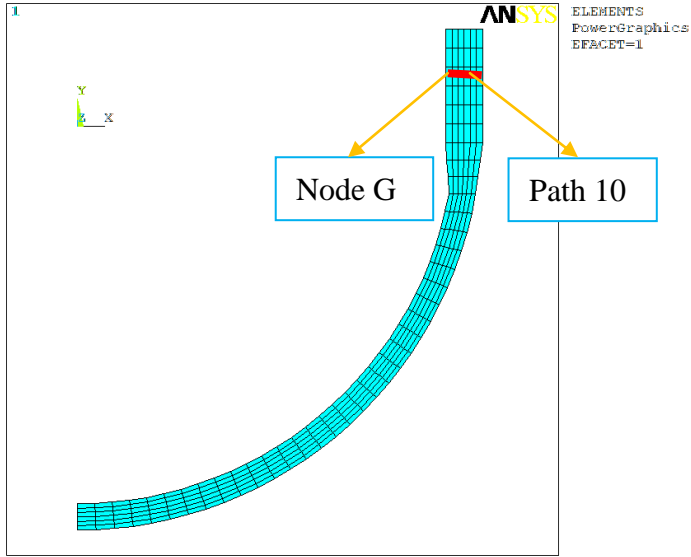


Fig. 76 Path 1 and Node A of 2-D model thermo-mechanical analysis for CASE 1

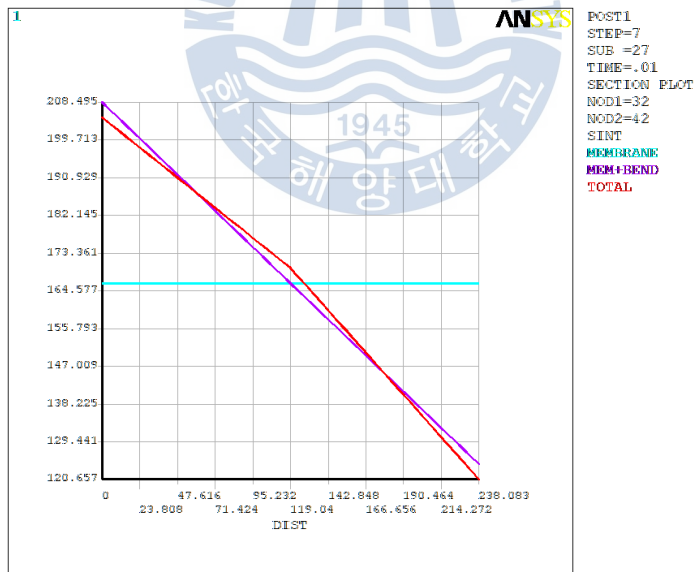


Fig. 77 Membrane and membrane plus bending stress at 0.01 sec along Path 10 of 2-D model thermo-mechanical analysis for CASE 1

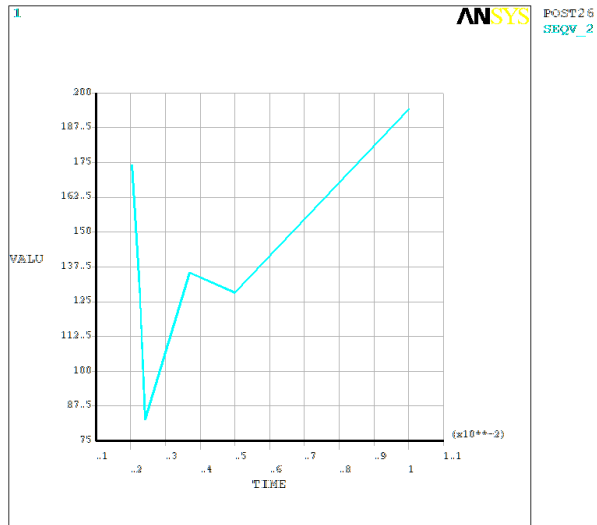


Fig. 78 Time history of equivalent stress at Node G of 2-D model thermo-mechanical analysis for CASE 1

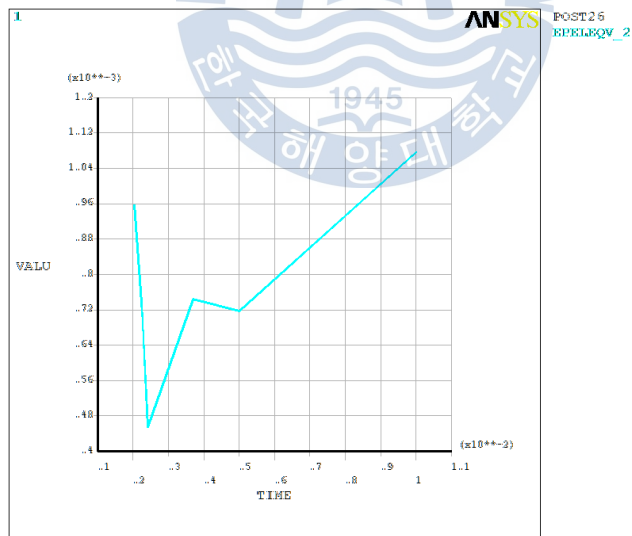


Fig. 79 Time history of equivalent strain at Node G of 2-D model thermo-mechanical analysis for CASE 1

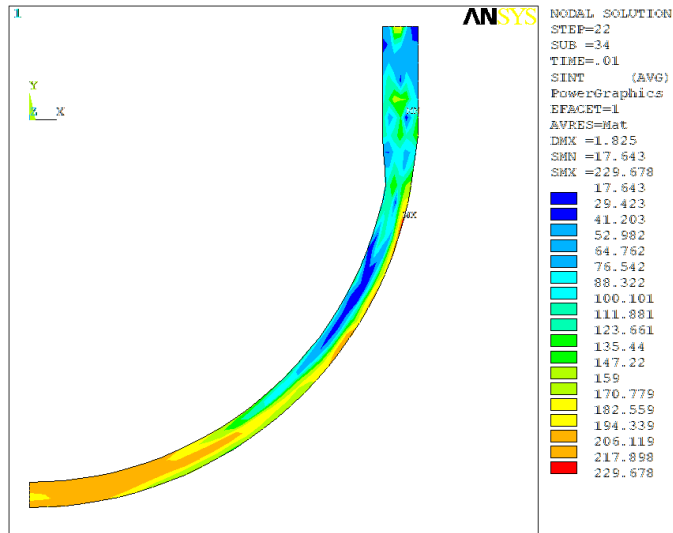


Fig. 80 Stress intensity distribution at 0.01 sec of 2-D model thermo-mechanical analysis
 for CASE 2

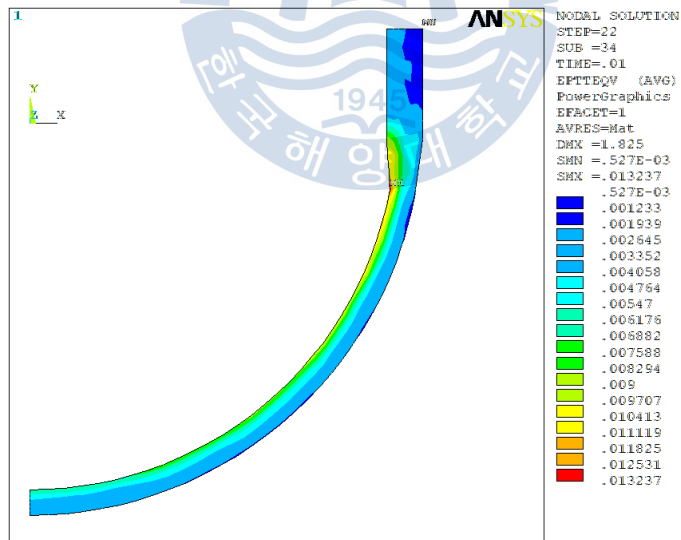


Fig. 81 Total strain distribution at 0.01 sec of 2-D model thermo-mechanical analysis for
 CASE 2

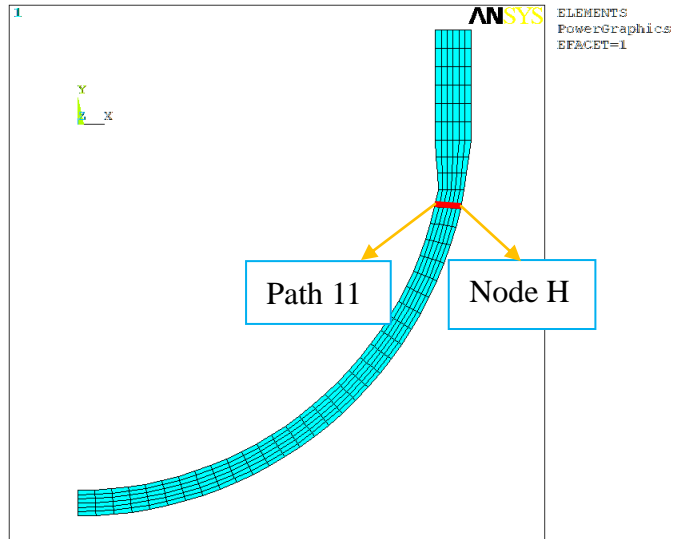


Fig. 82 Path 1 and Node A of 2-D model thermo-mechanical analysis for CASE 2

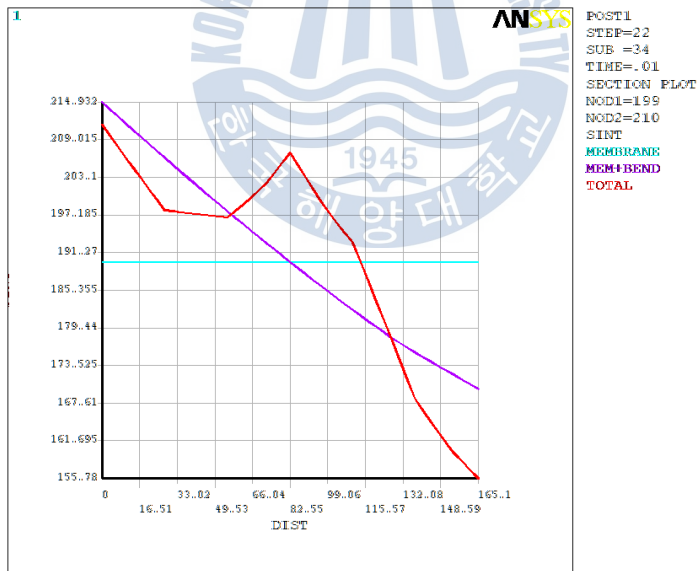


Fig. 83 Membrane and membrane plus bending stress at 0.01 sec along Path 11 of 2-D model thermo-mechanical analysis for CASE 2

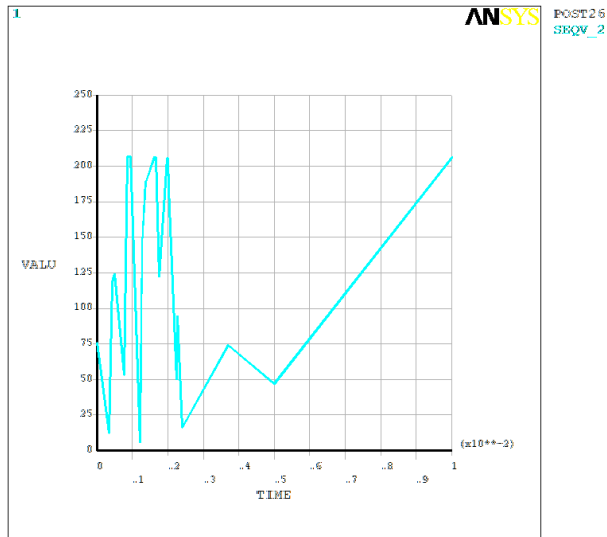


Fig. 84 Time history of equivalent stress at Node H of 2-D model thermo-mechanical analysis for CASE 2

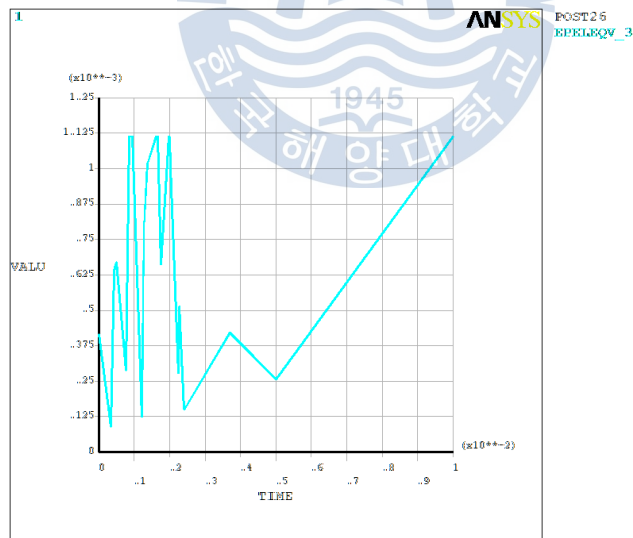


Fig. 85 Time history of equivalent strain at Node H of 2-D model thermo-mechanical analysis for CASE 2

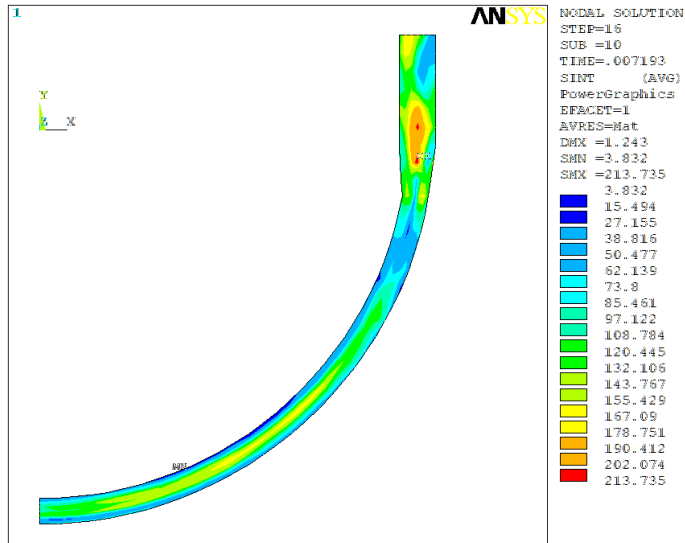


Fig. 86 Stress intensity distribution at 0.0072 sec of 2-D model thermo-mechanical analysis for CASE 3

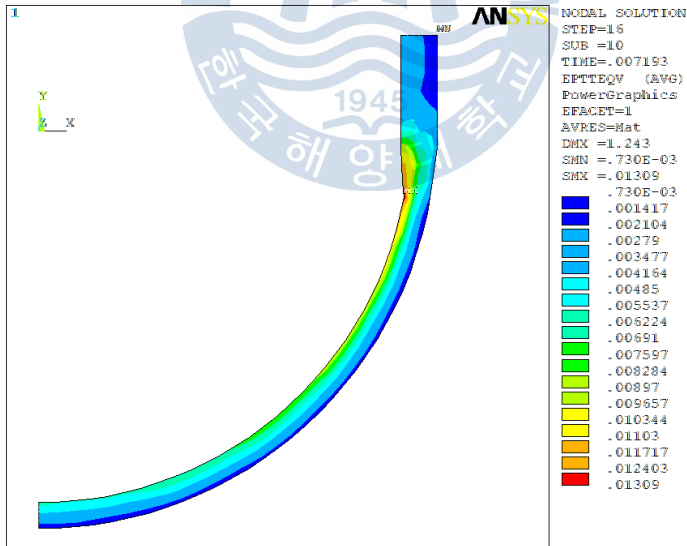


Fig. 87 Total strain distribution at 0.0072 sec of 2-D model thermo-mechanical analysis for CASE 3

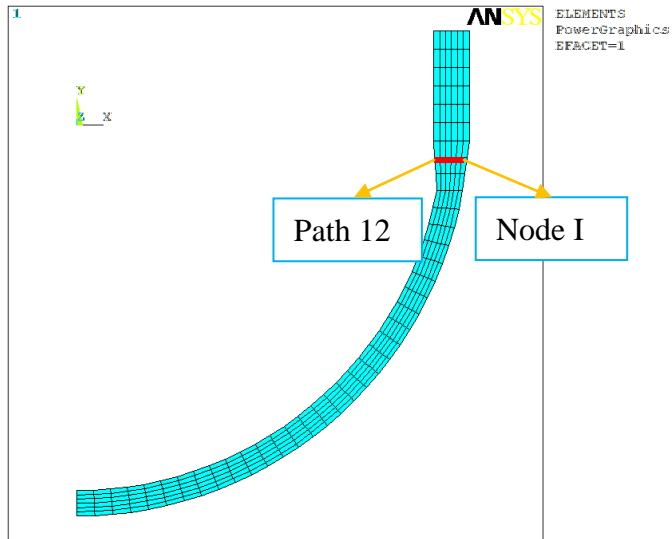


Fig. 88 Path 1 and Node A of 2-D model thermo-mechanical analysis for CASE 3

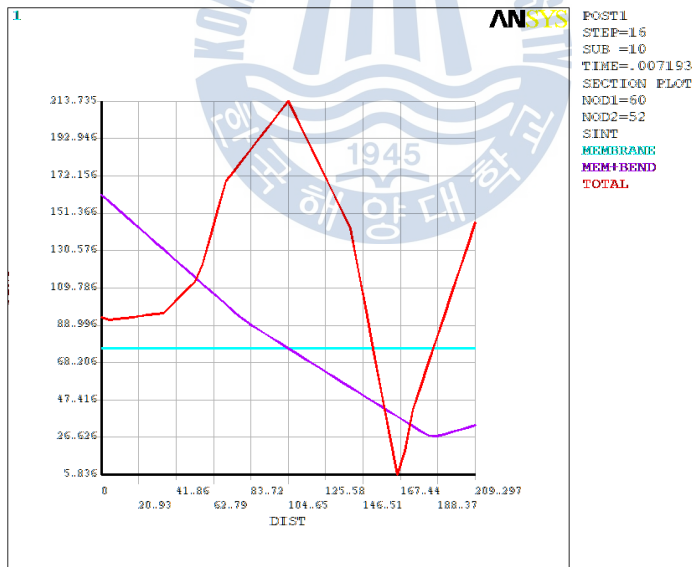


Fig. 89 Membrane and membrane plus bending stress at 0.0072 sec along Path 12 of 2-D model thermo-mechanical analysis for CASE 3

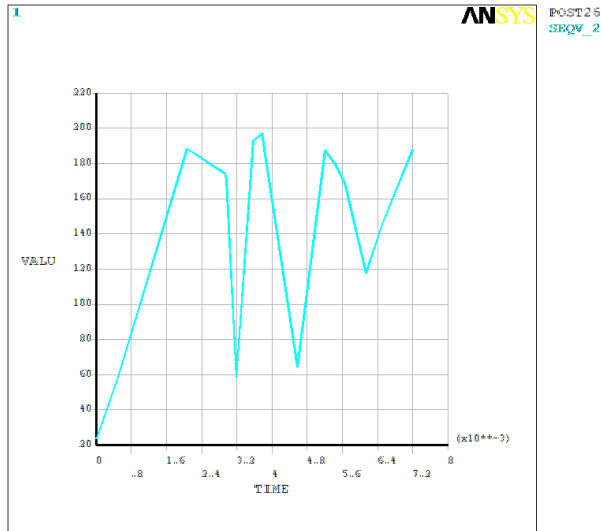


Fig.90 Time history of equivalent stress at Node I of 2-D model thermo-mechanical analysis for CASE 3

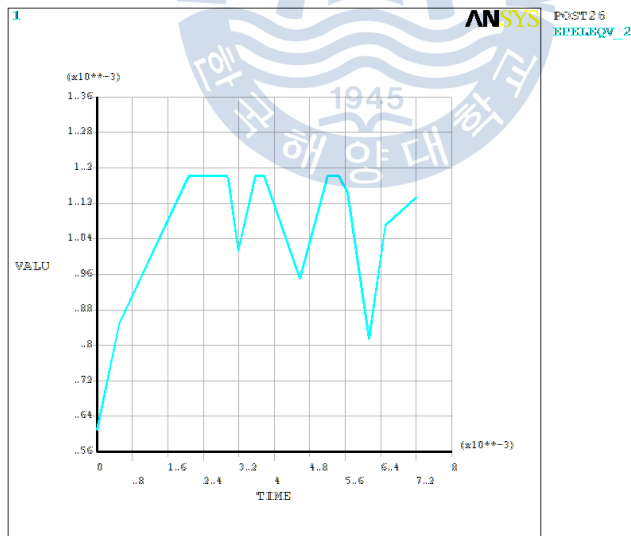


Fig. 91 Time history of equivalent strain at Node I of 2-D model thermo-mechanical analysis for CASE 3

4. Conclusion and Future Work

A safety assessment of the nuclear reactor lower head under in-vessel vapor explosion loads has been performed, two analysis methods are used: structural analysis and thermo-mechanical analysis. Firstly, the calculated explosion pressure loads are imposed on the lower head inner wall, strain calculations and membrane stress intensity are calculated by using ANSYS 11.0 program; secondly, both the calculated explosion pressure loads and the thermal loads are imposed on the modeling of the lower head, total strain and membrane stress intensity are calculated by using ANSYS 11.0 program. And then, the calculated strain and stress results are compared with the reference standard values of failure criteria to determine the failure of the lower head

The thermal analysis supplies the temperature distribution of the lower head, it must be analysed before the thermo-mechanical analysis, because the thermo-mechanical analysis is based on the thermal analysis.

Structural analysis results used the calculated pressure loads on the lower head inner wall show that the vapor explosion-induced lower head failure is physically unreasonable under the pressure value up to 118.5 MPa.

Thermo-mechanical analysis results used both pressure loads and thermal loads on the modeling of the lower head show that the vapor explosion-induced lower head failure also does not exist under the pressure value up to 118.5 MPa and the temperature value up to 700°C.

The thermal analysis results used the temperature convection loads on the lower head show that the boiling crisis does not exist under present situation.

In this paper, it's only considered the static thermal condition, however, the heat transfer process from the inside to outside of the lower head need some time to finish, the temperature of the lower head is different at different time. So in order to get a more

accurate analysis result, the transient thermal situation must be considered, which just as the time historical explosion pressure load.

For the thermo-structural analysis, the 2-D modeling of lower head is only considered instead of considering the 3-D modeling, in order to calculate the detail structural and welding condition just as the structural analysis, the 3-D modeling thermo-structural analysis is the future work to complete, and then a more accurate and comprehensive result will be obtained.



References

- [1] 박광연, 조종래, 박익규, 최병욱, 김기용, 이경중, 1998, Technical report: Research & Development on Next Generation Reactor, Safety Assessment of In-Vessel Vapor Explosion Loads in Next Generation Reactor, 49-54.
- [2] ASME Boiler & Pressure Vessel Design Code Section III, ASME, 1995
- [3] W.R. Bohr and T.A. Butler, “Comments on Proposed Research Contributing to the Relation of Residual Steam Explosion Issues,” Letter Report in “A Review of Current Understanding of the Potential for Containment Failure Arising from In-vessel Steam Explosion,” NUREG-1116, U.S Nuclear Regulatory Commission, Feb. 1985.
- [4] M. Berman, D.V. Swenson and A.J. Eickett, “An Uncertainty Study of PWR Steam Explosions,” SAND83-1438, NUREG/CR-3369, Sandia National Laboratories, May 1984.
- [5] A.K. Ghosh, Metall. Trans., 7A, 523, 1976.
- [6] T.G. Theofanous, C. Liu, S. Additon, S. Angelini, O. Kymalainen, T. Salmassi, 1997, “In-Vessel coolability and retention of a core melt”, Nuclear Engineering and Design, 7-10.
- [7] B.R. Sehgal, A. Theerthan, A. Giri, A. Karbojian, H.G. Willschutz, O. Kymalainen, S. Vandroux, J.M. Bonnet and so on, 2003, “Assessment of reactor vessel integrity (ARVI), Nuclear Engineering and Design, 25-29.
- [8] Vincent Koundy, Cataldo Caroli, Laetitia Nicolas, Philippe Matheron, Jean-Marie Gentzbittel, Michel Coret, 2008, “Study of tearing behavior of a PWR reactor pressure vessel lower head under severe accident loadings”, Nuclear Engineering and Design, 1-5.
- [9] Vincent Koundy, Nguyen Hieu Hoang, 2008, “Modelling of PWR lower head failure

- under severe accident loading using improved shells of revolution theory”, Nuclear Engineering and Design, 2400-2406
- [10] T.L. Schulz, 2006, “Westinghouse AP1000 advanced passive plant”, Nuclear Engineering and Design, 1547-1553.
- [11] R. Krieg, B. Dolensky, B. Goller, G. Hailfinger, T. Jordan, G. Messemer, N. Prothmann, E. Stratmanns, 2003, “Load carrying capacity of a reactor vessel head under molten core slug impact”, “Final report including recent experimental findings”, Nuclear Engineering and Design, 241-243
- [12] T.G. Theofanous, W.W. Yuen, S. Angelini, J.J. Sienicki, K. Freeman, X. Chen, T. Salmassi, 1999, “Lower head integrity under steam explosion loads”, Nuclear Engineering and Design, 7-12
- [13] T.G. Theofanous, J.P. Tu, A.T. Dinh, T.N. Dinh, 2002, “The boiling crisis phenomenon Part I : nucleation and nucleate boiling heat transfer”, Experimental Thermal and Fluids Science, 775-782.

